Atmospheric
Chemistry
and Physics
Discussions

Open Access

Formation of highly oxidized multifunctional compounds: autoxidation of peroxy radicals formed in the ozonolysis of alkenes – deduced from structure–product relationships

T. F. Mentel[1], M. Springer[1], M. Ehn[1,2], E. Kleist[3], I. Pullinen[1], T. Kurtén[4], M. Rissanen[2], A. Wahner[1], and J. Wildt[3]

[1]Institut für Energie- und Klimaforschung, IEK-8, Forschungszentrum Jülich, Jülich, Germany
[2]Department of Physics, University of Helsinki, 00014 Helsinki, Finland
[3]Institut für Bio- und Geowissenschaften, IBG-2, Forschungszentrum Jülich, Jülich, Germany
[4]Department of Chemistry, University of Helsinki, 00014 Helsinki, Finland

ACPD

15, 2791–2851, 2015

Formation of highly oxidized multifunctional compounds

T. F. Mentel et al.

Title Page

Abstract	Introduction
Conclusions	References
Tables	Figures

|◄ | ►|

◄ | ►

Back | Close

Full Screen / Esc

Printer-friendly Version

Interactive Discussion

Abstract

It has been postulated that secondary organic particulate matter plays a pivotal role in the early growth of newly formed particles in forest areas. The recently detected class of extremely low volatile organic compounds (ELVOC) provides the missing organic vapours and possibly contributes a significant fraction to atmospheric SOA. ELVOC are highly oxidized multifunctional molecules (HOM), formed by sequential rearrangement of peroxy radicals and subsequent O_2 addition. Key for efficiency in early particle growth is that formation of HOM is induced by one attack of the oxidant (here O_3) and followed by an autoxidation process involving molecular oxygen. Similar mechanisms were recently observed and predicted by quantum mechanical calculations e.g. for isoprene. To assess the atmospheric importance and therewith the potential generality, it is crucial to understand the formation pathway of HOM.

To elucidate the formation path of HOM as well as necessary and sufficient structural prerequisites of their formation we studied homologues series of cycloalkenes in comparison to two monoterpenes. We were able to directly observe highly oxidized multifunctional peroxy radicals with 8 or 10 O-atoms by an Atmospheric Pressure interface High Resolution Time of Flight Mass Spectrometer equipped with a NO_3^--Chemical Ionization (CI) source. In case of O_3 acting as oxidant the starting peroxy radical is formed on the so called vinylhydroperoxide path. HOM peroxy radicals and their termination reactions with other peroxy radicals, including dimerization, allowed for analysing the observed mass spectra and narrow down the likely formation path. As consequence we propose that HOM are multifunctional percarboxylic acids, with carbonyl-, hydroperoxy-, or hydroxy-groups arising from the termination steps. We figured that aldehyde groups facilitate the initial rearrangement steps. In simple molecules like cyloalkenes autoxidation was limited to both terminal C-atoms and two further C-atoms in the respective α-positions. In more complex molecules containing tertiary H-atoms or small constraint rings even higher oxidation degree were possible, either

by simple H-shift of the tertiary H-atom or by initialisation of complex ring-opening reactions.

1 Introduction

The formation of new particles is an important process in the natural and anthropogenically influenced atmosphere (Kerminen et al., 2005; Kuang et al., 2009; Hamed et al., 2007; Kulmala et al., 2004a, 2013; Spracklen et al., 2010). While it seems now clear that sulfuric acid molecules, eventually in interaction with amines and ammonia, form the first nuclei (Bzdek et al., 2013; Berndt et al., 2005; Kuang et al., 2008; Sipälä et al., 2010; Vuollekoski et al., 2010; Zhao et al., 2011; Kirkby et al., 2011; Almeida et al., 2013), the mechanisms of growth of such nuclei has been under a debate for a long time (Kulmala et al., 2004b, 2013; Kerminen et al., 2010; Riccobono et al., 2012). Since new particle formation is often observed in forest regions with relatively clean air, the amount of sulfuric acid is insufficient to explain the observed growth and it has always been proposed that organic vapors should be involved in particle growth (Zhang et al., 2004; Metzger et al., 2010; Paasonen et al., 2010; Riipinen et al., 2011, 2012; Ehn et al., 2012, 2014; Riccobono et al., 2014; Schobesberger et al., 2013; Kulmala et al., 2013). The organic vapors were supposed to have very low vapor pressures and it was estimated that such vapors could make up more than 50 % of the organic fraction (Riipinen et al., 2011; Yli-Juuti et al., 2011). However, in the atmosphere volatile organic compounds (VOC) are emitted mainly as hydrocarbons or with low degree of oxidation, otherwise they would not be volatile. Organic molecules with the required degree of oxidation and functionalization to exhibit sufficiently low vapor pressures very often require several oxidation steps to be formed from VOC in the gas phase by OH radicals. Stepwise oxidation by OH radicals makes the overall oxidation process slow and/or would lead to a high degree of diversification of products, as OH is not a very specific oxidation agent. Such sequential oxidation is not suited to produce high supersaturations of organic vapors required for growing molecular size critical nuclei.

New instrumentation, namely the atmospheric pressure interface time-of-flight mass spectrometer (APi-TOF-MS, Junninen et al., 2010) enabled the direct measurement of natural ions in the atmosphere. By applying APi-TOF-MS in Hyytiälä, a forestry station in Southern Finland, Ehn et al. (2010) observed ions of organic compounds in mass ranges of 300–400 and 500–600 Da. They suggested at the time that these are highly oxidized organics, likely organic nitrates and their dimers. In a study in the Jülich Plant Atmosphere Chamber (JPAC) using APi-TOF-MS, Ehn et al. (2012) demonstrated that the organics observed in Hyytiälä mainly arise from α-pinene ozonlysis; the mass spectrometric pattern derived for β-pinene and isoprene were different than that from α-pinene. The JPAC is operated as continuously stirred flow reactor (Mentel et al., 2009) and the steady state can be conserved for an arbitrary duration. This allowed for long integration times and application of the low sensitivity but high resolution W-mode of APi-TOF-MS. This way Ehn et al. (2012) determined that the compounds seen in the mass spectra in JPAC and Hyytiälä are highly oxidized C_{10}-compounds clustered with NO_3^- and the respective dimers, also clustered with NO_3^-. The C_{10} compounds exhibit O/C ratios close to one or larger and a number of H-atoms similar to the reactand α-pinene (H_{14} or H_{16}), resulting in molecular formulas $C_{10}H_{14,16}O_{9-11}$. Similar organic molecules were observed independently in the CLOUD studies in cluster with sulfuric acid (Schobesberger et al., 2013).

The C_{10} compounds in question are highly oxidized multifunctional molecules (HOM, Ehn et al., 2012) and thus must have very low vapor pressures. They have been also called extremely low volatile organic compounds (ELVOC, Schobesberger et al., 2013; Ehn et al., 2014) in order to account for their role in the early stage of new particle formation and to distinguish them from other volatility classes such as low volatile organic compounds (LVOC), semi volatile organic compounds (SVOC), and intermediate volatile organic compounds (IVOC) which are discussed in atmospheric formation of secondary organic aerosol (SOA) (Donahue et al., 2012; Jimenez et al., 2009; Murphy et al., 2014). We focus here on the structure and chemistry of ELVOC and not so much on their atmospheric role in particle formation as extreme low volatility condensable

Title Page

Abstract | Introduction

Conclusions | References

Tables | Figures

◀ | ▶

◀ | ▶

Back | Close

Full Screen / Esc

Printer-friendly Version

Interactive Discussion

organic vapors. We will therefore use the notation HOM (highly oxidized multifunctional molecules, Ehn et al., 2012) when referring to chemical structures and pathways and use the notation ELVOC, when referring to the impacts in the atmosphere.

By making use of the fact that ELVOC prefer to cluster with NO_3^-, Ehn et al. (2014) applied NO_3^--CI-APi-TOF-MS (Jokinen et al., 2012) and demonstrated that the formation of ELVOC is significant with a branching ratio of $7\% \pm 3.5\%$ of the turnover of α-pinene with ozone. Moreover, it seems that endocyclic double bonds in monoterpenes like limonene are structural features that support ELVOC formation (Ehn et al., 2014; Jokinenen et al., 2014). Further, it was suggested that a radical chain of peroxy radical formation and intramolecular H-shifts could be the path to ELVOC formation, resulting in multiple hydroperoxides with increasing oxygen content in steps of 32 Da (Ehn et al., 2014). H-migration to peroxy radicals is known at elevated temperatures and for specific atmospheric radicals (Cox and Cole, 1985; Glowacki and Pilling, 2010) and the mechanism is commensurable with recent findings for the autoxidation of isoprene and related compounds (Crounse et al., 2012, 2013, 2011) and with quantum-mechanical calculations, regarding the oxidation of monoterpenes (Vereecken and Francisco, 2012; Nguyen et al., 2010; Peeters et al., 2009; Vereecken et al., 2007). Jokinen et al. (2014) demonstrated HOM formation in detail for limonene, a monoterpene. The detailed chemistry of HOM formation from cyclohexene was elucidated by Rissanen et al. (2014). In this study we investigated experimentally which structural and functional elements in organic molecules favor HOM formation initiated by ozonolysis.

In the studies by Ehn et al. (2014, 2012) HOM with odd number of H-atoms were detected, suggesting that highly oxidized peroxy radicals were observed. This observation was recently confirmed by Rissanen et al. (2014) and Jokinen et al. (2014). By increasing NO in the system the peroxy radicals behaved as expected from classical atmospheric chemistry: their concentration decreased as did the concentration of dimer structures and in turn organic nitrates increased (Ehn et al., 2014). As we will show in the following chapters, the peroxy radicals are indeed the pivotal point to understanding HOM formation. By comparing HOM formation of selected model and representative

Title Page

Abstract | Introduction

Conclusions | References

Tables | Figures

|◄ | ►|

◄ | ►

Back | Close

Full Screen / Esc

Printer-friendly Version

Interactive Discussion

(cc) BY

compounds with specific structural properties we will deduce routes to highly oxidized multifunctional molecules, making use of established features of ozonolysis and termination reactions of peroxy radicals, together with the rearrangement of peroxy radicals by H-shift from C-H to $>COO^\bullet$ groups.

2 Experimental

All experiments were carried out in the Jülich Plant Atmospheric Chamber (JPAC). Details of the set-up are described in Mentel et al. (2009) and Ehn et al. (2014). The largest chamber, with a volume of 1450 L, was used in the experiments presented here and it was operated as a continuously stirred flow reactor. Temperature (T = 17 °C) and relative humidity (RH = 60 %) were held constant during the experiments. Two changes were implemented in the 1450 L reactor since Mentel et al. (2009): the whole UV lamp assembly is now placed in a 100 mm diameter quartz tube flanged in across the chamber from wall to wall, in order to reduce direct contact of the reaction mixture with the warm UV-lamp surface. On top of the Teflon floor of the chamber a glass floor was placed on 10 mm spacers in order to reduce fluorinated compounds and memory effects of HNO_3 detected by Ehn et al. (2012). By pumping away the air in the space between Teflon plate and glass plate at a flow rate of $1.5\,L\,min^{-1}$ diffusion of fluorinated compounds into the chamber was diminished.

Supply air was pumped through the chamber at a total flow of $30–35\,L\,min^{-1}$ resulting in a residence time of 40–50 min. The supply flow was split in two different lines for the reactants in order to prevent reactions in the supply lines. Ozone and water vapor was added to one of the air streams entering the reaction chamber, while the other inlet stream contained the volatile organic compound (VOC) of interest. The individual VOC were taken from diffusion sources which are described in Heiden et al. (2003). The hydrocarbons investigated in this study are listed in Table 1 together with their molecular mass, purity and supply information. The steady state concentrations of the VOC during the experiments are given in Table 1. Independent of the VOC added to

the chamber, the ozone flow into the reaction chamber was held constant. As a consequence the steady state O_3 concentrations varied depending on the reactivity of added hydrocarbons with respect to O_3 as given in Table 1. All experiments were performed under low NO (NO < 30 ppt) and low NO_2 (NO_2 < 300 ppt) conditions.

The central analytical instrument was an Atmospheric Pressure interface High Resolution Time of Flight Mass Spectrometer (APi-TOF-MS, Aerodyne Research Inc. and Tofwerk AG; Junninen et al., 2010). The APi-TOF-MS was equipped with a NO_3^--Chemical Ionization (CI) source (Eisele and Tanner, 1993; Jokinen et al., 2012; A70 CI-inlet, Airmodus Ltd) for the detection of highly oxidized organic compounds. The reagent ion $^{15}NO_3^-$ for the CI was generated by using labeled $H^{15}NO_3$ (~ 10N in H_2O, 98 atom % ^{15}N, Aldrich Chemistry), ionized by an in-line ^{241}Am foil. As was shown by Ehn et al. (2012) the anion NO_3^- is able to form a cluster with the expected highly oxidized organic compounds. The labeling with $^{15}NO_3^-$ enables to distinguish between ^{15}N from the reagent and ^{14}N that has been incorporated into the sample molecules, e.g. through reactions with ^{14}NO in the reaction chamber.

The sampling flow from the reaction chamber into the CI source was $10\,L\,min^{-1}$. The flow into the APi-TOF-MS was thereafter reduced to $0.8\,L\,min^{-1}$ by passing a critical orifice. Differential pumping by a scroll pump and a three-stage turbo pump sequentially decreased the pressure from 10^3 mbar in the CI region to 10^{-6} mbar in the Time of Flight region. Once the ions are sampled into the APi-TOF region, they are guided by segmented quadrupole mass filters and electrical lenses in the TOF extraction region. Collisions between ions and gas molecules will take place, but the energies are tuned low enough that only weakly bound clusters (e.g. water clusters) will fragment. After extraction into the TOF the ions are separated by their different flight times depending on their mass to charge ratio.

The sensitivity of the APi-TOF operated as NO_3^--CIMS is discussed in Ehn et al. (2014). We have indication that once a certain degree of functionalization is achieved (two –OH or –OOH groups in addition to two carbonyl groups) the sensitivity is fairly the same for all HOM species (Mikael Ehn, Theo Kurten, personal commu-

Formation of highly oxidized multifunctional compounds

T. F. Mentel et al.

Title Page

Abstract	Introduction
Conclusions	References
Tables	Figures

|◄ | ►|

◄ | ►

Back | Close

Full Screen / Esc

nication). HOM with 6 or less C atoms and less than 6 O-atoms were not detected. However, we found hints that we may be able to detect HOM with less than 6 O-atoms in molecules with 7 or more C-atoms. Thus, the general polarizibility of a molecule may play a role besides directed interactions of functional groups with the NO_3^- ion.

5   To control whether or not peaks in the APi-TOF mass spectra originated from oxidation of the added VOC, blank experiments without VOC addition were performed. Ozone was left in the chamber in case of peaks originating from ozonolysis of impurities. Some of the peaks in the mass spectra were abundant also in absence of VOC and likely arise from fluorinated contaminants. All peaks observable without VOC addition

10 were rejected from interpretation.

    Ozonolysis of alkenes in the dark produces OH radicals. We did not use OH scavenger in most of our experiments. However, in some control experiments OH produced during alkene-ozonolysis was scavenged by adding ~ 40 ppm carbon monoxide (CO). Addition of CO did not change the majority of the patterns in the mass spectra in-

15 dicating that ozonolysis was indeed the major pathway of HOM formation under the experimental conditions. Nevertheless, CO addition changed the abundance of certain HOM. This was used to separate OH reactions as origin for these HOM.

3   Methods

The goal of this section is to derive an a priori expectation scheme for formation of

20 highly oxidized molecules from ozonolysis of VOC with endocyclic double bonds, and to predict which intermediates and termination products should be formed according to classical understanding and recent mechanistic developments. As we will show, comparison of the expectations to the observed mass spectra (positive hits) will make it easier to identify and organize the observations. Of course the scheme was developed

25 a posteriori but presenting it beforehand will help the reader to follow the argumentation.

Under our experimental conditions the ozonolysis is the major pathway of alkene oxidation. In case of alkenes with endocyclic double bonds ozonolysis leads to ring opening with a Criegee intermediate at one end of the carbon chain and a carbonyl group on the other end. The Criegee intermediate further reacts in several ways. One of these is the so-called vinylhydroperoxide pathway (Reactions R1–R3, see Sequence 1). The decomposition of the vinylhydroperoxides (Reaction R2) leads to a radical with mesomeric structures (S1, see Sequence 1). Importantly here, the peroxy radical S2 is formed by subsequent O_2 addition to the oxo-alkyl mesomeric structure (Reaction R3) (cf. reviews of Johnson and Marston, 2008 and Vereecken and Francisco, 2012).

Peroxy radical S2 is the starting point of the following considerations. As shown in Sequence 2 in general, the reaction chain can be terminated by the known reactions of the peroxy radicals (denoted as RO_2) with HO_2 (Reaction R4), with other peroxy radicals (Reactions R5 and R8), or with NO (Reaction R7b) leading to termination products with hydroperoxy, carbonyl, or hydroxy groups, alkylperoxides, or organic nitrates. The chain can also be continued by peroxy-peroxy (Reaction R6a) and peroxy-NO (Reaction R7a) reactions via alkoxy intermediates. The latter form carbonyl compounds (Reaction R6b) or fragment into smaller units (e.g. Vereecken and Francisco, 2012). In addition, alkoxy radicals can undergo isomerization reactions like the H-shift with subsequent O_2 addition (see Sequence 3, Vereecken and Francisco, 2012; Vereecken and Peeters, 2010). Note, that the peroxy functionality is recycled in Sequence 3, generating OH-functionalized peroxy radicals hydroxy-peroxy radicals can be terminated in the usual way (Sequence 2). All these principle pathways are either known (e.g. Finlayson-Pitts and Pitts Jr., 2000) or have been recently discussed, based on either calculations (e.g. Vereecken and Francisco, 2012) and/or observations for C_5 VOC (e.g. Crounse et al., 2013).

We will also allow for H-shifts from C-H bonds also in peroxy radicals (Sequence 4), leading to –OOH functionalized peroxy radicals (Crounse et al., 2013; Vereecken et al., 2007). This rearrangement was known for processes at elevated temperatures (Cox and Cole, 1985; Glowacki and Pilling, 2010), but has not been considered as

important in gas-phase atmospheric chemistry until recently. In addition intramolecular termination Reaction (R9c) can occur, an H-shift from the C-H bond that carries the hydroperoxy group, leading to a split off of OH and a carbonyl termination product (Crounse et al., 2013; Rissanen et al., 2014). Sequence 4 explains the mass increase in steps of 32 Th in the type of HOM observed by Ehn et al. (2012, 2014) and investigated here. Since it requires only a single attack by the oxidant O_3 and then proceeds by itself under involvement of only molecular oxygen, it can be interpreted as an autoxidation process.

We will apply the known steps (Reactions R4–R6, Sequence 2) and rearrangement and autoxidation of peroxy radicals (Sequences 4 and 3) to construct a pathway to form atmospheric HOM which is in accordance with both, our mass spectral observations and experimental findings as well as the quantum mechanical calculations by Rissanen et al. (2014). Since we were working at low NO_x (< 300 ppt) and under conditions of negligible NO_2 photolysis we will neglect the NO pathways (Reaction R7, Sequence 2).

In this study we will focus on such pathways where the peroxy radicals and their termination products retain the carbon number of the reactants. These are the majority of the observed products. In addition, we will consider their dimers with twice the number of C-atoms (Reaction R8, Sequence 2).

As we will show, most of the observed HOM arise from the straight peroxy autoxidation path (Sequence 4), which we will denote as peroxy path. However, often a minor fraction of products arises from Sequence 3, which we will call the hydroxy-peroxy path. Peroxy radicals arising from the hydroxy-peroxy path are OH substituted and contain an *odd* number of O-atoms (like S3 in Sequence 3). The hydroxy-peroxy radical can carry on the autoxidation (Sequence 4) and terminate in usual ways (Reactions R4–R6 and R8 in Sequence 2).

Applying the principles outlined above to the example of cyclopentene, we may expect from the *peroxy path* the type of species in Table 2a; possible intermediates and products from *hydroxy-peroxy path* are shown in Table 2b. According to the vinylhy-

Title Page

Abstract | Introduction

Conclusions | References

Tables | Figures

|◄ | ►|

◄ | ►

Back | Close

Full Screen / Esc

Printer-friendly Version

Interactive Discussion

droperoxide path the *starting* peroxy radical in the series (upper left corner of Table 2a) is a C_5 chain with aldehyde functions on both ends. In addition a peroxy radical function is located at the C-atom in α-position to one of the aldehyde groups: S2 with $R = (CH_2)_2$ (see Sequence 1).

5   Radical S2 is the *starting* point for either further H-shift/O_2 addition (Table 2a, down the first column) or termination products (along the line). The scheme does not explain the relative importance of the pathways, only that they could be a priori possible. In reality, the abundances of stable termination products and postulated peroxy radicals are the result of detailed local molecular structure and a complex formation and destruction
10   scheme as discussed below (individual lifetimes, cf. Rissanen et al., 2014). Moreover, our detection method may require a certain minimum degree of oxidation of the analyte molecules before they can be detected as nitrate clusters. The parent peroxy radicals with molecular mass m and their termination products form a repeated pattern $m - 17$ (carbonyl), $m - 15$ (hydroxy), m, $m + 1$ (hydroperoxy) in the mass spectra. This is
15   indicated in second line of Table 2a.

The first entrée in Table 2b is a hydroxy-peroxy radical of type S3 which is formed by Sequence 3 from the starting intermediate S2 in Table 2a. The hydroxy-peroxy radicals noted in the first column of Table 2b can be either formed by Sequence 3 from the corresponding peroxy radicals noted in the first column of Table 2a or in increments of
20   O_2 by H-shift/O_2 addition (Sequence 4) of the previous hydroxy-peroxy radical.

It is evident from Table 2 that both peroxy and hydroxy-peroxy pathways generate progressions in the mass spectra with distance 32 Da (2xO). However, the two progressions are shifted by 16 (the O of the hydroxy group in the hydroxy-peroxy radical) with respect to each other. This can lead to isobaric overlap of hydroperoxides ($m + 1$)
25   from the peroxide m and hydroxy termination products from the corresponding hydroxy-peroxide at $m + 16$ ($m + 16$–15, cf. column 4 in Table 2a and column 3 in Table 2b).

We investigated several compounds to detect structural prerequisites of the formation of HOM. The cyclic alkenes cyclopentene, cyclohexene, and cycloheptene were used to study the impact of chain length on HOM formation. 1-methyl-cyclohexene

was used to study possible impacts of methyl-substitution of the double bond, with structural similarity to α-pinene. In 3-methyl-cyclohexene and 4-methyl-cyclohexene the methyl substituent is moving away from the endocyclic double bond, and they provide branched C_7 variations of cycloheptene.

Finally, we studied the formation of HOM from the functionalized linear alkenes (Z)-6-nonenal, (Z)-6-nonenol, (5)-hexen-2-one, and 1-heptene. These compounds were chosen because during ozonolysis they should produce a peroxy radical function located in α-position to the forming aldehyde group (similar to S2, Sequence 1), but carry a different or none functional group at the other, the terminal or ω-C-atom, end of the chain. The reason was to study the impact of a functionalization on atmospheric HOM formation. Two monoterpenes, α-pinene and Δ-3-carene, both abundant in nature, serve as test cases for atmospherically relevant, complex bicyclic molecules. α-pinene and Δ-3-carene carry tertiary H-atoms, as do 3-methyl-cyclohexene and 4-methyl-cyclohexene.

4   Results

Closed shell HOM and their peroxy intermediates were detected as clusters with one $^{15}NO_3^-$ ion attached (Ehn et al., 2012, 2014). Note that the postulated peroxy radicals have odd molecular masses because of the missing hydrogen atom, but due to the use of ^{15}N labeled nitric acid to generate $^{15}NO_3^-$ as reagent ion they will be detected as $^{15}NO_3^-$-cluster at even masses. In the same sense all closed shell molecules will be detected as $^{15}NO_3^-$-clusters at odd masses.

Figure 1 shows a typical mass spectrum observed for cyclopentene ozonolysis in range between 240 and 280 Th which is where the nitrate clusters of C_5-HOM are expected. It shows that we indeed observe the set of termination products as developed in Sect. 3. In addition, we found a peak at 258 Th to which we attributed the molecular formula $C_5H_7O_8 \cdot NO_3^-$. This cluster has an odd number of H-atoms indicating that the organic moiety is not a closed shell molecule. As we will show in the following

Title Page

Abstract | Introduction

Conclusions | References

Tables | Figures

|◀ | ▶|

◀ | ▶

Back | Close

Full Screen / Esc

Printer-friendly Version

Interactive Discussion

chapter, this indeed is the peroxy radical. The corresponding termination products are indicated by their mass difference to the peroxy radical at $m = 258$ Th, as introduced in the Method section. The signal at 273 Th is the carbonyl termination product from the next progression shifted by 32 Th. The peak at 255 Th is a cluster with a perfluorinated acid (chamber artefact).

Figure 2 shows the same mass spectrum in the region of dimer structures. The two largest peaks at 421 and 389 Th have organic moieties with molecular formulas $C_{10}H_{14}O_{14}$ and $C_{10}H_{14}O_{12}$, which we will attribute to peroxides formed by recombination of peroxy radicals. The molecular formulas assigned to the peaks at 343 and 375 Th contain 16 H-atoms and odd number of oxygen ($C_{10}H_{16}O_9$, $C_{10}H_{16}O_{11}$) and the compounds are obviously formed on a different formation path. As we did not quench OH radicals also formed in the vinyl hydroperoxide path, oxidation by OH may be involved in the formation of these compounds.

Similar mass spectrometric patterns were observed for all investigated compounds that form HOM and Table 3 gives the overview which of the compounds formed HOM in our ozonolysis experiments. In Table 3 we also list the functionalization at the ω-C-atom, the opposite end of the initial peroxy radical, as explained by structures S2, S4a, S4b, and S5-S7 in Fig. 3. In case of methyl-substituted double bonds the symmetry is broken and the initial peroxy radical can be either formed at the unsubstitued site of the double bond, then the ω-terminal group is a acetyl group (S5) or at the substituted site (S4a, b) then the ω-terminal group is an aldehyde. In case of the linear alkenes, we consider only the product with the longer C-chain after ozonolysis of the double bond. The peroxy group resides in α-position to the remaining C-atom of the double bond leaving the ω-terminal group to whatever was at the other end of the parent molecule.

Efficient formation of highly oxidized molecules was found for the ozonolysis of all endocyclic alkenes, including α-pinene and Δ-3-carene, and from ozonolysis of (Z)-6-nonenal. In contrast ozonolysis of 1-heptene, (Z)-6-nonenol and 5-hexen-2-on did *not* lead to substantial formation of highly oxidized molecules. In all the positive cases the mass spectra were dominated by few peaks, analogous to Figs. 1 and 2, and these

are listed in Tables 4–10, 12, and 13. All these compounds have in common that the respective starting peroxy radicals of type S2 or S4a, b in Fig. 3 can be formed.

The absence of highly oxidized molecules of 1-heptene, (Z)-6-nonenol, and especially 5-hexen-2-on suggests that an *aldehyde group* at the ω-C-atom facilitate HOM formation. No functionality (CH$_3$-), a methyl-oxo group CH$_3$-C(=O)-, or an alcohol group HO-CH$_2$- at the ω-end of the molecule obviously do not strongly promote formation of HOM. The positive results for 1-methyl-cyclohexene, and both monoterpenes (MT) indicate that the peroxy radical group can be located either in α-position to a keto- or an aldehyde group. Applying our scheme, this means that ω–aldehyde functionality in peroxy radicals S2 and S4a, b in Fig. 3 favors H-shifts, while the other groups in S5–S7 do not.

5 Discussion

5.1 Unsubstituted cycloalkenes, peroxy radicals, and (Z)-6-nonenal

Tables 4–6 list the molecular masses of the organic moieties that were attributed to highly oxidized molecules, derived from the mass spectra for the cases of cyclopentene, cyclohexene, and cycloheptene. The mass of the nitrate ion was subtracted and termination products of peroxy radicals with mass m were classified as by $m - 17$ (carbonyl), $m - 15$ (hydroxy) and $m + 1$ (hydroperoxy), as in Table 2 of the Method section. Only such molecular structures that were indeed observed are noted, together with their molecular mass and the precise m/z at which the molecules were detected as cluster with NO$_3^-$. Clearly, we did not found all possible intermediates and termination products derived in the Method section.

As shown already in Fig. 1, we often observed quite strong peaks at such odd masses m where we would expect the peroxy radicals. From the molecular formula alone, which is assessable by APi-TOF-MS, their chemical character as alkyl-, alkoxy- or peroxy radicals cannot be distinguished. Alkoxy and alkyl radicals react with the

O_2 in air, while peroxy radicals react mainly with other peroxy radicals or NO, the latter being low in our experiments. We can exclude alkyl and alkoxy radicals, as their lifetime is too short to allow for formation in measurable amounts (and to survive in the APi-TOF-MS). Other candidates would be organic nitrates, which we exclude by the observed mass defects and because of our low NO_x conditions. Moreover, highly oxidized nitrates would be expected at $m + 30$, so they cannot interfere with O or O_2 progressions of m. A contribution of ^{13}C isotope can be excluded if there is no strong signal at $m - 1$. We conclude that the strong peaks at m are peroxy radicals. It is known that peroxy radicals can have lifetimes of minutes (e.g., Finlayson-Pitts and Pitts Jr., 2000, Sect. 6.D.2.e), so they can be built up in high enough concentrations and obviously survive in our APi-TOF-MS. HOM peroxy radicals were also observed in previous studies (Ehn et al., 2014; Jokinen et al., 2014; Rissanen et al., 2014). However, in case of a significant contribution of the hydroxy-peroxy path leading to hydroxy-peroxy radicals at $m + 16$ the corresponding carbonyl termination product resides at the $m - 1$ ($m + 16$–17) position. In these cases the ^{13}C contribution of the carbonyl termination product at m must be considered and corrected.

According to the scheme in Table 2, the starting point for formation of highly oxidized molecules is the peroxy radical of type S2 (Sequence 1) with $R = (CH_2)_{2-4}$ and four O-atoms. The first detected peroxy radicals were $C_5H_7O_8$, $C_6H_9O_8$, and $C_7H_{11}O_8$ and the most oxidized were the O_{10}-analogues (Tables 4–6). Peroxy radicals with odd oxygen numbers likely involve alkoxy rearrangement Sequence 3 at one step. We will discuss both findings later in detail.

The next columns in Tables 4–6 list the stable HOM produced in termination reactions from the peroxy radical in the first column. All intensities were normalized to the strongest signal. For cyclohexene and cycloheptene this is the O_9-carbonyl termination product ($m - 17$) which is formed from the peroxy radical carrying ten O-atoms either via Reactions (R5) and (R6) (Sequence 2) or, as shown by Rissanen et al. (2014), via Reaction (R9c) (Sequence 4). The corresponding peak is second largest for cyclopentene; here the O_7-carbonyl termination product from the precursor peroxy radical with

Title Page

Abstract | Introduction

Conclusions | References

Tables | Figures

|◀ | ▶|

◀ | ▶

Back | Close

Full Screen / Esc

Printer-friendly Version

Interactive Discussion

eight O-atoms is about a factor of two larger (Table 4). The analogous product appeared also for cyclohexene, however contributing only 20 % of the largest carbonyl termination product (Table 5), and it is unimportant for cycloheptene (Table 6). In general carbonyl termination products ($m - 17$) arising from Reactions (R5) and (R6) are expected to be the major products under low NO$_x$ (i.e. atmospheric) conditions.

Compared to carbonyl termination products, hydroxy ($m - 15$) and hydroperoxy termination products ($m + 1$) are less important termination products and only for cyclopentene we find significant contribution of hydroxy and hydroperoxy termination products of 10–20 %. Their contribution is decreasing with increasing chain length, and their contribution in case of cycloheptene is less than 1 %. Increasing chain length may making the geometry of the H-shift more favourable (i.e. 1,6 instead of 1,5 or 1,4 etc). Thus, the H-shifts of longer-chain peroxy radicals become faster, while bimolecular reactions are more or less unchanged, thus giving more carbonyl termination products in relation to hydroxy and hydroperoxy termination products. The detailed product distribution must be also dependent on the reaction conditions, i.e. reactand and oxidant concentrations, temperature etc. For example the formation of hydroperoxy groups is controlled by HO$_2$/RO$_2$ ratio and we did not take specific measures to hold this ratio constant.

For cyclopentene the hydroperoxide C$_5$H$_8$O$_8$ provides a substantial contribution of 19 % under the given conditions. C$_5$H$_8$O$_8$ can be either the hydroperoxy termination product from C$_5$H$_7$O$_8$ + HO$_2$ (Reaction R4) or an hydroxy termination product formed in reaction (Reaction R5, Sequence 2) including the hydroxy-peroxy radical C$_5$H$_7$O$_9$. Both lead to same isobaric mass (Table 4). Since the corresponding carbonyl termination product is missing and the precursor C$_5$H$_7$O$_9$ of the hydroxy termination product is much less abundant than that of the hydroperoxy product C$_5$H$_7$O$_8$, we suggest that the main fraction of the peak observed for C$_5$H$_8$O$_8$ is the hydroperoxy termination prodcuct.

As is obvious from Tables 4 and 5, for cyclopentene and cyclohexene, only molecules with more than seven oxygen atoms were detected. However, as can be seen in Table 6 for cycloheptene, five or less O-atoms can be detected for C$_7$ compounds, but only in

Title Page

Abstract | Introduction

Conclusions | References

Tables | Figures

|◄ | ►|

◄ | ►

Back | Close

Full Screen / Esc

Printer-friendly Version

Interactive Discussion

traces. This is corroborated by Table 7 for (Z)-6-nonenal and Tables 8 and 9 for the methyl-cyclohexenes.

We can already deduce some rules for formation of HOM from the results of cyclopentene, cyclohexene and cycloheptene and construct a mechanistic scheme as shown in Fig. 4 (cf. Rissanen et al., 2014). The most abundant peaks in the monomer range of HOM can be attributed to products preserving the C-atom number of the precursor. They form regular patterns in the mass spectra, which can be explained by expected termination products of RO_2 termination reactions Sequence 2 and the intramolecular termination Reaction (R9c) (Rissanen et al., 2014), either directly via the peroxy path Sequence 4 or via an alternative, the hydroxy-peroxy path, involving alkoxy rearrangement Sequence 3 as intermediate step.

Stable, closed shell termination products are most abundant. Carbonyl termination products (S8, S11) are more abundant than hydroperoxy (S10, S13) and hydroxy termination products (S9, S12, S14) and all together they are more abundant than the peroxy radicals. Products of the hydroxy-peroxy path gain importance with increasing chain length, but remain sparse and less abundant than products from the peroxy path. Independent of the chain length the maximum number of oxygen atoms observed in peroxy radicals and hydroperoxides is ten, or nine for corresponding carbonyl and hydroxy termination products, because here one O atom is lost in termination Reactions (R5) and (R6a) (Sequence 2). The starting radicals S2 have 4 O-atoms – two carbonyl end groups (2 × O) and a peroxy functionality (1 × OO•) in α-position to one of the end groups. Therefore, the H-shift/O_2-addition mechanism of peroxy radicals can operate up to 3 times introducing up to 6 further O-atoms. This together with the sensitivity of formation of highly oxidized molecules to an aldehyde ω-terminal group (Table 3) suggest that easy H-shift is limited to the two terminal C-atoms and the two C-atoms in α-position to them. The H-atoms of the aldehyde groups are relative weakly bound (Rissanen et al., 2014) and so it is not surprising that they are preferably attacked as shown in the first steps on the left hand side in Fig. 4. (Additional constraints are the steric availability of the H-atoms.) In general the binding energy of an H-atom to

a carbon atom depends on the functional group added to the respective C-atom. Low binding energies certainly will favor H-shifts (given a suited geometry) and therefore favor the autoxidation mechanism (e.g. Glowacki and Pilling, 2010).

Attack on aldehyde H-atom leads to peroxy radicals of type $-C(=O)OO^•$ and after further H-shift to percarboxylic acid groups $-C(=O)OOH$ (Fig. 4). We suggest that percarboxylic acid groups are o able to activate the H-atoms at their neighbor C-atom in α-position. This will support one more autoxidation step. Termination here can lead to the dominant carbonyl termination products. From these observations we deduce that a highly oxidized carbonyl compound should have the structure S11 in Fig. 4, i.e. a di-percarboxylic acid with hydroperoxide group and keto group, both in α-position to the percarboxylic acid groups, at least in the case of the plain cycloalkenes discussed here. Assuming that a percarboxylic acid group is required for H-shift activation at its neighboring α-C-atom the corresponding hydroperoxy and hydroxy termination products should look like structures S12 and S10 in Fig. 4.

If the percarboxylic group is able to activate the H-atoms at its α-C-atom to be competitive with a shift of an aldehyde-H, the final attack could also occur at the aldehyde group. This would lead to either S13 under hydroperoxy termination or to the structure S14, a mixed carboxyl percarboxylic di-acid with hydroperoxide groups at the C-atoms in α-position of the acid functions, isobaric to S12 in Fig. 4.

Our interpretations are corroborated by the findings for (Z)-6-nonenal. Ozonolysis of (Z)-6-nonenal leads to either a C_3-Criegee intermediate and a C_6-dialdehyde, or propanal and a C_6-Criegee intermediate. Via the vinylhydroperoxide path the latter forms the same starting peroxy radical as the ring opening of cyclohexene. Indeed, two peroxy radicals were detected for (Z)-6-nonenal and the dominant peak is the carbonyl termination product from the O_{10}-peroxy radical (Table 7).

5.2 Methyl substitution of cyclohexene

In order to support the suggested reaction path to HOM in Fig. 4, we now will investigate the effect of methyl substitution of the double bond. This is also one step fur-

ther towards α-pinene, the most abundant MT, which forms ELVOC in the atmosphere (Ehn et al., 2012, 2014). Table 8 lists the results for 1-methyl-cyclohexene. Here the largest peak is the carbonyl termination product $C_7H_{10}O_7$ arising from the peroxy radical $C_7H_{11}O_8$. The corresponding O_7-hydroxy and O_7-hydroperoxy termination products can be also identified. As in the case of cycloheptene, highly oxidized molecules with less than seven O-atoms are detectable, but in very small amounts only. Compared to cycloheptene (and cyclohexene) the HOM arising from the O_8 peroxy radical dominate while termination products from the O_{10} peroxy radical are sparse.

The methyl substitution at the double bond introduces asymmetry, leading to three different vinylhydroperoxides and three different starting peroxy radicals S15–S17 (Fig. 5).The peroxy radical S17 in Fig. 5 has a methyl-oxo and *not* an aldehyde group as ω-terminal group. In case of 5-hexen-2-on only the S17 analog, S5, (Fig. 3) is formed and 5-hexen-2-on did not undergo HOM formation. Peroxy radicals in S15 and S16 (Fig. 5) can rearrange under H-shift from the ω-aldehyde group and subsequent O_2 addition. S15 and S16 are similar with only the hydroperoxide group at different positions. According to the scheme developed here this should lead to the same set of isobaric products, and for clarity we will only follow the fate of peroxy radical S15. In case of S15 the autoxidation mechanism would lead to peroxy radical S18 and in a further step to peroxy radical S19. S19 terminates in the usual way or intramolecular (Reaction R9c) to either ketones (S20, S21) or a hydroxy product (S22), or a hydroperoxide (S23). The isobaric carbonyl termination products (S20, S21) are by far the largest contribution in the spectrum, as hydroxy and hydroperoxy termination products contribute only about 1–2 % in total. It is notable that the maximum oxidation is indeed limited to 7/8 O-atoms, two less compared to the major termination products of cycloheptene.

The products of 3- and 4-methyl-cyclohexene (Tables 10 and 11), as well as cycloheptene (Table 6) show similar patterns. Methyl substitution leads only to minor variations of the cycloheptene HOM pattern with the 3-methyl-hexene being little more deviant. This could indicate steric effects, which fade if the methyl group moves away

from the double bond, i.e. away from the molecule ends of the ring opening products susceptible to H-shifts.

Table 9 compares the HOM of all C_7 cycloalkenes investigated. As discussed, 1-methyl substitution leads to unique HOM pattern wherein the highest oxidation step is only very weakly expressed. This is likely caused by the fact that the ring opening for 1-methyl cyclohexene leads only to one aldehyde group, instead of two as for cyclo-heptene, 3-methyl-cyclohexene, and 4-methyl-cyclohexene.

In case of 4-methyl cyclohexene (Table 11) we find small contributions of $C_7H_{10}O_{11}$ indicating that in complex molecules higher degrees of oxidation may be achieved. We hypothesize, that the tertiary H-atom at the methyl branching may be susceptible to H-shift of peroxy groups. The observation of the O_{11}-carbonyl termination products suggests that the attack on the tertiary H-atom is not necessarily the final step, as tertiary peroxy radicals cannot stabilize into ketones. If several H-atoms are susceptible to H-shift of peroxy groups – with different rates – permutation of pathways will occur according to the respective rate coefficients. For 3-methyl-cyclohexene the effect of the tertiary peroxy radicals is not so distinct, because the methyl group resides on the α-C-atom next to an aldehyde group from which we expect H-shift anyhow.

5.3 Monoterpenes and tertiary H-atoms

Tables 12 and 13 show the result for two bicyclic MT, α-pinene (cf. Ehn et al., 2014) and Δ-3-carene. Both MT contain the same methyl-substituted 6-ring structure as 1-methyl cyclohexene. In case of 1-methyl cyclohexene we are quite confident that the highest peroxy radical should look like S19 in Figs. 5 and 6. If we *construct* the analogous per-oxy radicals for α-pinene and Δ-3-carene they should look like S24 and S25 in Fig. 6, so the maximum oxidation degree in analogy to the cycloalkenes should be limited as for 1-methyl-cyclohexene, i.e. either bimolecular or intramolecular termination.

Comparison shows that for the MT higher oxidation degrees were achieved (Tables 12 and 13). While for 1-methyl cyclohexene the major termination product is a ke-tone with seven O-atoms, α-pinene and Δ-3-carene generate substantial amounts of

ketones with nine (α-pinene, Δ-3-carene) or even 11 (α-pinene) O-atoms. While for simple cycloalkenes carbonyl termination products dominate (Tables 4–8), the major termination products of α-pinene and 3-carene appear at the m/z of the corresponding to hydroxy termination with nine O-atoms (presumably four OOH groups), and α-pinene also generates the next higher hydroxy termination product with 11 O-atoms (see Tables 12 and 13).

As already indicated for 4-methyl cyclohexene, which shows HOM with 11 O-atoms, H-shift from tertiary C-atoms can obviously lead to a spread of formation routes (tertiary H-atoms shown in Fig. 6). So far, MT molecules are too complex to guess the pathways only from the observed mass spectra. However, the fact that the dominant MT termination products are hydroxy rather than carbonyl compounds indicates that alkoxy involving steps maybe more important for MT than for the simpler alkenes and that ring opening of the cyclobutyl/propyl rings is involved in HOM formation (Rissanen et al., 2015). A relative gain in hydroxy and hydroperoxy termination products is also commensurable with a higher number of peroxy radicals at tertiary C-atoms, which cannot form ketones via H-abstraction by air oxygen. Please note, that although the oxidation degree is higher than to be expected from our formation scheme for plain C_5–C_7 cycloalkenes, the mass spectrometric pattern of peroxy-radical with $m/z = m$, carbonyl $m - 17$, hydroxy $m - 15$, hydroperoxy $m + 1$ still applies and helps to order the analysis of the mass spectra. We conclude that the routes to HOM for simple molecules proposed by us are basic but not sufficient to explain HOM formation in complex molecules.

5.4 Dimers and peroxyradicals

Besides HOM with the same number of C-atoms as the precursor, we observe also HOM molecules with twice the C-atom numbers of the precursors, thus having dimer character. Table 14 lists the detected and assigned HOM dimers from cyclopentene, which had the highest chemical turnover (due to the fastest rate coefficient and the largest O_3 concentration). The peak intensities were normalized to the dominant dimer.

Title Page

Abstract | Introduction

Conclusions | References

Tables | Figures

|◀ | ▶|

◀ | ▶

Back | Close

Full Screen / Esc

Printer-friendly Version

Interactive Discussion

The two most abundant dimers contain even number of O-atoms and 14 H-atoms. But we found also dimers with 16 H-atoms and odd number of O-atoms.

Since we observe the peroxy radicals directly it is suggestive to test if the dimers are peroxides and arise from recombination of two peroxy radicals according to Reaction (R8) (Sequence 2). We assume that two peroxy radicals recombine to a peroxide under elimination of O_2. Table 15 lists the dimers expected for cyclopentene by simply permuting all observed and some additional peroxy radicals (those with less O-substitution, which we expect but probably are not detectable for cyclopentene). The molecular formulas of dimers which were observed are marked in bold face. The most abundant, identified peroxy radicals (compare Table 4) are also marked in bold face.

The dimer with the largest signal has the molecular formula $C_{10}H_{14}O_{14}$, and it can be formed by reaction of two $C_5H_7O_8$, the dominant peroxy radical (cf. Table 4). But it is also clear that several combinations of peroxy radical pairs can lead to dimers with the same molecular mass. Formulas in Table 15 set in bold face and italic indicate dimers which involve the two most abundant peroxy radicals. We also detect dimers which comprise the involvement of low O precursors (Table 15 first line, normal face). This is indicative of their existence, although due to instrument limitations we probably are not able to detect them. Not all combinations are of the same likelihood. For example, $C_{10}H_{14}O_{16}$ is less likely formed by dimerization of $C_5H_7O_9$, which would arise from the minor hydoxy-peroxy path, but more likely by recombination of $C_5H_7O_8$ and $C_5H_7O_{10}$. Of course each combination of suited peroxy radical pairs may contribute somewhat to the observed dimer. The findings of $C_{10}H_{14}O_{12,14,16}$ dimers in Table 14 mutually support our assignments of peroxy radicals as well as our assignments of dimers. It overall supports the basic formation schemes developed in the Method section.

Notably, there are still the two dimers in Table 14 with odd numbers of oxygen atoms which contain 16 H-atoms. Due to the 16 H-atoms these dimers cannot be simply formed by any combination of the peroxy radicals detected during cyclopentene ozonolysis, which carry only seven H-atoms. However, the $C_{10}H_{16}O_9$ dimer may be formed as a re-combination of the most abundant $C_5H_7O_8$ peroxy radical and a peroxy radical with

the molecular formula $C_5H_9O_3$. In the same way $C_{10}H_{16}O_{11}$ dimers could be formed by the observed $C_5H_7O_{10}$ peroxy radical and the $C_5H_9O_3$ peroxy radical. $C_5H_9O_3$ is the molecular formula of the first peroxy radical in the oxidation chain of cyclopentene by OH. Production of the $C_5H_9O_3$ peroxy radical from cyclopentene occurs via OH addi-

5 tion to one site of the double bond and addition of O_2 at the other site, which is an alkyl radical site. Reactions with OH are possible since we did not routinely quench dark OH in the ozonolysis experiments.

As first peroxy radical in the OH-oxidation chain of cyclopentene, the $C_5H_9O_3$ peroxy radical should be quite abundant. Due to the low number of O atoms in this radical it

10 is not detectable with our APi-TOF-MS scheme. To test the hypothesis of OH reactions being involved in the formation of these dimers, CO was added as OH scavenger (∼ 40 ppm) in a cyclopentene ozonolysis control experiment. Figure 7 shows the overlay of the dimer spectra from cyclopentene ozonolysis with and without CO addition.

CO addition led indeed to a decrease in the abundance of both H_{16}-HOM dimers

15 detected at 343 and 375 Th, suspected to arise from te $C_5H_9O_3$ peroxy radical. Furthermore, the abundance of $C_{10}H_{14}O_{12}$ (detected at 389 Th) and that of $C_{10}H_{14}O_{14}$ (detected at 421 Th) increased. This is in accordance with suppression of the competition by $C_5H_9O_3$ from cyclopentene + OH reaction. After suppression of OH more ozonolysis products in general and more dimers by ozonolysis-only products are formed, e.g.

20 $C_5H_7O_8 + C_5H_7O_8$.

Moreover, there are more peaks which decrease by CO addition. This means, that these molecules likely involve oxidation by OH radicals at some step. It's noticeable that all peaks that decrease can be attributed to dimer structures containing an odd number of oxygen atoms (the reagent ion $^{15}NO_3^-$ substracted). In contrast dimer structures

25 which contain an even number of oxygen atoms increase under CO addition, indicating that their formation involve ozonolysis-only products.

In the monomer region, the addition of CO should increase the relative contribution of hydroperoxide termination products since quenching with CO converts OH to HO_2 molecules, thus increasing the HO_2 concentration. This would be a further support of

our assignment of peroxy radicals and their termination products but deserves more detailed investigations.

5.5 Role of the hydroxy peroxy path

As can be seen from the Tables 4–10, 12 and 13, peroxy radicals with even numbers of O-atoms were often observed. In contrast peroxy radicals with odd numbers of O atoms as well as their termination products were only rarely found. We hypothesize, that peroxy radicals with odd numbers of O-atoms can be formed from alkoxy radicals that undergo an H-shift (Vereecken and Peeters, 2010), and thereby form the alkyl radical to which the O_2 is added. Their low abundance can be understood applying basic steady state considerations. H-shifts of alkoxy radicals (Reaction R6c) formed in Reaction (R6a), and subsequent O_2 addition (Reaction R6d), has to compete with the termination Reaction (R6b), if the alkoxy C-atom carries an H-atom. As O_2 concentrations are very high, the chemical lifetime of an alkoxy radical is much shorter than that of a peroxy radical. This also presupposes that the consecutive addition of molecular oxygen after H-shifts in peroxy radicals is highly efficient.

6 Summary and conclusions

A key to our analysis was the direct observation of highly oxidized peroxy radicals in oxidations initiated by ozone. As to be expected in atmospheric oxidation processes, peroxy radicals were the pivotal point to elucidate the pathways of HOM formation and therewith the pathways to atmospherically relevant ELVOC. Peroxy radicals are formed in ozonolysis via the vinylhydroperoxide pathway, and are sequentially oxidized by rearrangement (H-shift) and subsequent addition of moelcular oxygen, renewing the peroxy radical at the next level of oxidation (Ehn et al., 2014; Rissanen et al., 2014). Since only a single initial oxidation step by ozone is required and thereafter oxidation

Title Page

Abstract | Introduction

Conclusions | References

Tables | Figures

|◄ | ►|

◄ | ►

Back | Close

Full Screen / Esc

Printer-friendly Version

Interactive Discussion

proceeds perpetuating a peroxy radical under addition of air oxygen alone, this process can be conceived as autoxidation of the peroxy radicals.

By our experimental studies of HOM formation using selected molecules with systematically varying structural properties, we deduced important steps on the route to HOM formation during ozonolysis. Peroxy radicals are formed via the vinylhydroperoxide path. Initially, aldehyde functionality facilitates the shift of an H-atom from a C–H bond to a peroxy radical group $> COO^{\bullet}$. As a consequence peroxy-carboxyl radicals are formed, which on further H-shift reactions form percarboxylic acid groups. These are able to activate the H-atoms on their neighbor α-C atom. Thus, in the ozonolysis of simple endocyclic alkenes up to 10 O-atoms can be incorporated in a peroxy radical, of those 6 O-atoms by the sequential autoxidation mechanism. We conclude that intermediates with two aldehyde end groups form di-percarboxylic acids with further carbonyl, hydroxy or hydroperoxide functionalities. We observed that presence of tertiary H-atoms by methyl substitution or constraint ring structures, like for α-pinene and Δ-3-carene, leads to more options for the autoxidation mechanism to proceed. This is allowing for addition of more than six O-atoms (here eight O-atoms) and a widening of the termination product spectrum.

An aldehyde group at the ω-end of the initial peroxy radical S2 favors the achievement of the highest oxidation degree. In the cases investigated here, methyl, hydroxy and keto groups are not efficient in promoting H-shift of C–H bonds at neighboring α-C-atoms to peroxy groups. The 1,4 H-shift from the aldehyde group to the peroxy radical in those molecules (S5–S7) may lead to a hydroperoxide, percarboxylic acid or hydroperoxy carboxylic acid, but then likely the autoxidation stops. If such molecules are formed, we may not be able to detect them with the NO_3^--APi-TOF-MS. A key finding for the role of ω-substitution is that (Z)-6-nonenal is forming the same major HOM as cyclohexene (Rissanen et al., 2014).

In the first few steps, as long as H-atoms susceptible to H-shift are available, autoxidation can compete with the termination reactions. At later stages termination reactions become more important and carbonyl, hydroxy, and hydroperoxy termination products

Title Page

Abstract	Introduction
Conclusions	References
Tables	Figures

|◀ | ▶|

◀ | ▶

Back | Close

Full Screen / Esc

Printer-friendly Version

Interactive Discussion

are formed in our NO poor system. Self-reactions of the HOM peroxy radicals lead to another class of dimer termination products, very likely peroxides. The elemental composition and relative abundance of the dimer structures indicate involvement of the monomer peroxy radicals of all oxidation stages in their formation. The most abundant dimers always involve the most abundant peroxy radicals. In addition we found dimers from the most abundant HOM peroxy radicals with the O_3-peroxy radicals formed in the first step after attack addition of OH to the double bond. These disappeared when OH was quenched by CO. In general quenching with CO suppresses the OH pathways and shifts termination towards HOO, as would be expected. Overall the mass spectrometric patterns of termination products and dimer formation support the pivotal role of highly oxidized peroxy radicals and that we indeed observe them directly.

We observe peroxy radicals with an odd number of oxygen, however, during ozonolysis their concentration were minor. The observations of peroxy radicals with an odd number of oxygen can be explained by the same concepts if we allow for a side pathway involving one intermediate step of alkoxy rearrangement (H-shift in an alkoxy radical, thereby formation of an alkyl radical and O_2 addition).

Considering the degree of oxidation as well as the functional groups in HOM, monomers and even more so dimers must have very low vapor pressures. Thus, HOM must play as ELVOC an important role in particle formation and SOA condensation (Ehn et al., 2014). The estimated molecular yields of ELVOC for α-pinene of 7 % (Ehn et al., 2014) and cyclcohexene of 4 % (Rissanen et al., 2014) indicate that ELVOC formation is in any case a minor part from the viewpoint of gas-phase chemistry. However, considering molar yields of a few percent and the high degree of oxidation, a substantial part of atmospheric SOA mass should be formed from ELVOC. The organic fraction of particles at early stages of formation should consist nearly exclusively of ELVOC (Ehn et al., 2014).

Actually, in JPAC we earlier observed linear growth curves in SOA formation, which we did not understand at the time. A characteristic of those experiments was that particle formation was induced based on relatively low BVOC input and in presence of the

Title Page

Abstract | Introduction

Conclusions | References

Tables | Figures

◄ | ►

◄ | ►

Back | Close

Full Screen / Esc

Printer-friendly Version

Interactive Discussion

BVOC-ozonolysis products (Mentel et al., 2009; Lang Yona et al., 2010). SOA growth curves of quasi non-volatile reaction products should be linear as Raoult's law does not apply and everything condenses. (The SOA yield curves were still curved as there was threshold before particle formation started, Mentel et al., 2009.)

An open question is the fate of HOM in the particulate phase. It seems obvious that the multifunctional HOM will not survive but undergo condensation reactions. The products of those are probably not retrievable by thermo-evaporation methods. It also raises the question how HOM based SOA relates to recently discussed glassy state of SOA particles (Koop et al., 2011; Shiraiwa et al., 2013; Virtanen et al., 2010; Zobrist et al., 2008).

We are confident that we deduced the main route of atmospheric oxidation that leads to "quasi" instantaneous formation of highly oxidized organic molecules. We are also confident that we deduced the major functionalization of HOM. Of course in our deductions there are still positive gaps (observations which we cannot explain with our current concepts) and negative gaps (missing structures that we would expect). But even at that level it is evident that formation of HOM is likely a general phenomenon, which was overlooked until very recently. To fully explore the general impact of HOM we need also to understand the role of OH oxidation and how the chemical systems behave at reasonably high NO_x concentrations. CI-APi-TOF-MS constitutes an enormous progress as it allows for unambiguous determination of the molecular formulas of HOM in laboratory experiments. However, for detailed mechanism development one would need also structural information and quantification of (all) intermediates and products is highly efficient

The service charges for this open access publication

Formation of highly oxidized multifunctional compounds

T. F. Mentel et al.

Title Page

Abstract | Introduction

Conclusions | References

Tables | Figures

◄ | ►

◄ | ►

Back | Close

Full Screen / Esc

Printer-friendly Version

Interactive Discussion

have been covered by a Research Centre of the Helmholtz Association.

References

Almeida, J., Schobesberger, S., Kuerten, A., Ortega, I. K., Kupiainen-Maatta, O., Praplan, A. P., Adamov, A., Amorim, A., Bianchi, F., Breitenlechner, M., David, A., Dommen, J., Donahue, N. M., Downard, A., Dunne, E., Duplissy, J., Ehrhart, S., Flagan, R. C., Franchin, A., Guida, R., Hakala, J., Hansel, A., Heinritzi, M., Henschel, H., Jokinen, T., Junninen, H., Kajos, M., Kangasluoma, J., Keskinen, H., Kupc, A., Kurten, T., Kvashin, A. N., Laaksonen, A., Lehtipalo, K., Leiminger, M., Leppa, J., Loukonen, V., Makhmutov, V., Mathot, S., McGrath, M. J., Nieminen, T., Olenius, T., Onnela, A., Petaja, T., Riccobono, F., Riipinen, I., Rissanen, M., Rondo, L., Ruuskanen, T., Santos, F. D., Sarnela, N., Schallhart, S., Schnitzhofer, R., Seinfeld, J. H., Simon, M., Sipilä, M., Stozhkov, Y., Stratmann, F., Tome, A., Troestl, J., Tsagkogeorgas, G., Vaattovaara, P., Viisanen, Y., Virtanen, A., Vrtala, A., Wagner, P. E., Weingartner, E., Wex, H., Williamson, C., Wimmer, D., Ye, P., Yli-Juuti, T., Carslaw, K. S., Kulmala, M., Curtius, J., Baltensperger, U., Worsnop, D. R., Vehkamaki, H., and Kirkby, J.: Molecular understanding of sulphuric acid-amine particle nucleation in the atmosphere, Nature, 502, 359–363, doi:10.1038/nature12663, 2013.

Berndt, T., Böge, O., Stratmann, F., Heintzenberg, J., and Kulmala, M.: Rapid formation of sulfuric acid particles at near-atmospheric conditions, Science, 307, 698–700, doi:10.1126/science.1104054, 2005.

Bzdek, B. R., Horan, A. J., Pennington, M. R., DePalma, J. W., Zhao, J., Jen, C. N., Hanson, D. R., Smith, J. N., McMurry, P. H., and Johnston, M. V.: Quantitative and time-resolved nanoparticle composition measurements during new particle formation, Faraday Discuss., 165, 25–43, doi:10.1039/c3fd00039g, 2013.

Cox, R. A. and Cole, J. A.: Chemical aspects of the autoignition of hydrocarbon-air mixtures, Combust. Flame, 60, 109–123, doi:10.1016/0010-2180(85)90001-x, 1985.

Crounse, J. D., Paulot, F., Kjaergaard, H. G., and Wennberg, P. O.: Peroxy radical isomerization in the oxidation of isoprene, Phys. Chem. Chem. Phys., 13, 13607–13613, doi:10.1039/c1cp21330j, 2011.

Title Page

Abstract | Introduction

Conclusions | References

Tables | Figures

|◄ | ►|

◄ | ►

Back | Close

Full Screen / Esc

Printer-friendly Version

Interactive Discussion

Crounse, J. D., Knap, H. C., Ornso, K. B., Jorgensen, S., Paulot, F., Kjaergaard, H. G., and Wennberg, P. O.: Atmospheric fate of methacrolein. 1. Peroxy radical isomerization following addition of OH and O_2, J. Phys. Chem. A, 116, 5756–5762, doi:10.1021/jp211560u, 2012.

Crounse, J. D., Nielsen, L. B., Jorgensen, S., Kjaergaard, H. G., and Wennberg, P. O.: Autoxidation of organic compounds in the atmosphere, J. Phys. Chem. Lett., 4, 3513–3520, doi:10.1021/jz4019207, 2013.

Donahue, N. M., Trump, E. R., Pierce, J. R., and Riipinen, I.: Theoretical constraints on pure vapor-pressure driven condensation of organics to ultrafine particles, Geophys. Res. Lett., 38, L16801, doi:10.1029/2011gl048115, 2011.

Donahue, N. M., Kroll, J. H., Pandis, S. N., and Robinson, A. L.: A two-dimensional volatility basis set – Part 2: Diagnostics of organic-aerosol evolution, Atmos. Chem. Phys., 12, 615–634, doi:10.5194/acp-12-615-2012, 2012.

Ehn, M., Junninen, H., Petäjä, T., Kurtén, T., Kerminen, V.-M., Schobesberger, S., Manninen, H. E., Ortega, I. K., Vehkamäki, H., Kulmala, M., and Worsnop, D. R.: Composition and temporal behavior of ambient ions in the boreal forest, Atmos. Chem. Phys., 10, 8513–8530, doi:10.5194/acp-10-8513-2010, 2010.

Ehn, M., Kleist, E., Junninen, H., Petäjä, T., Lönn, G., Schobesberger, S., Dal Maso, M., Trimborn, A., Kulmala, M., Worsnop, D. R., Wahner, A., Wildt, J., and Mentel, Th. F.: Gas phase formation of extremely oxidized pinene reaction products in chamber and ambient air, Atmos. Chem. Phys., 12, 5113–5127, doi:10.5194/acp-12-5113-2012, 2012.

Ehn, M., Thornton, J. A., Kleist, E., Sipilä, M., Junninen, H., Pullinen, I., Springer, M., Rubach, F., Tillmann, R., Lee, B., Lopez-Hilfiker, F., Andres, S., Acir, I.-H., Rissanen, M., Jokinen, T., Schobesberger, S., Kangasluoma, J., Kontkanen, J., Nieminen, T., Kurten, T., Nielsen, L. B., Jorgensen, S., Kjaergaard, H. G., Canagaratna, M., Maso, M. D., Berndt, T., Petaja, T., Wahner, A., Kerminen, V.-M., Kulmala, M., Worsnop, D. R., Wildt, J., and Mentel, T. F.: A large source of low-volatility secondary organic aerosol, Nature, 506, 476–479, doi:10.1038/nature13032, 2014.

Eisele, F. L. and Tanner, D. J.: Measurement of the gas-phase concentration of H_2SO_4 and Methane sulfonic acid and estimates of H_2SO_4 production and loss in the atmosphere, J. Geophys. Res.-Atmos., 98, 9001–9010, doi:10.1029/93jd00031, 1993.

Finlayson-Pitts, B. J. and Pitts Jr., J. N.: Chemistry of the Upper and Lower Atmosphere, Academic Press, San Diego, 2000.

Glowacki, D. R. and Pilling, M. J.: Unimolecular reactions of peroxy radicals in atmospheric chemistry and combustion, Chem. Phys. Chem., 11, 3836–3843, doi:10.1002/cphc.201000469, 2010.

Hamed, A., Joutsensaari, J., Mikkonen, S., Sogacheva, L., Dal Maso, M., Kulmala, M., Cavalli, F., Fuzzi, S., Facchini, M. C., Decesari, S., Mircea, M., Lehtinen, K. E. J., and Laaksonen, A.: Nucleation and growth of new particles in Po Valley, Italy, Atmos. Chem. Phys., 7, 355–376, doi:10.5194/acp-7-355-2007, 2007.

Jimenez, J. L., Canagaratna, M. R., Donahue, N. M., Prevot, A. S. H., Zhang, Q., Kroll, J. H., DeCarlo, P. F., Allan, J. D., Coe, H., Ng, N. L., Aiken, A. C., Docherty, K. S., Ulbrich, I. M., Grieshop, A. P., Robinson, A. L., Duplissy, J., Smith, J. D., Wilson, K. R., Lanz, V. A., Hueglin, C., Sun, Y. L., Tian, J., Laaksonen, A., Raatikainen, T., Rautiainen, J., Vaattovaara, P., Ehn, M., Kulmala, M., Tomlinson, J. M., Collins, D. R., Cubison, M. J., Dunlea, E. J., Huffman, J. A., Onasch, T. B., Alfarra, M. R., Williams, P. I., Bower, K., Kondo, Y., Schneider, J., Drewnick, F., Borrmann, S., Weimer, S., Demerjian, K., Salcedo, D., Cottrell, L., Griffin, R., Takami, A., Miyoshi, T., Hatakeyama, S., Shimono, A., Sun, J. Y., Zhang, Y. M., Dzepina, K., Kimmel, J. R., Sueper, D., Jayne, J. T., Herndon, S. C., Trimborn, A. M., Williams, L. R., Wood, E. C., Middlebrook, A. M., Kolb, C. E., Baltensperger, U., and Worsnop, D. R.: Evolution of organic aerosols in the atmosphere, Science, 326, 1525–1529, doi:10.1126/science.1180353, 2009.

Johnson, D. and Marston, G.: The gas-phase ozonolysis of unsaturated volatile organic compounds in the troposphere, Chem. Soc. Rev., 37, 699–716, doi:10.1039/b704260b, 2008.

Jokinen, T., Sipilä, M., Junninen, H., Ehn, M., Lönn, G., Hakala, J., Petäjä, T., Mauldin III, R. L., Kulmala, M., and Worsnop, D. R.: Atmospheric sulphuric acid and neutral cluster measurements using CI-APi-TOF, Atmos. Chem. Phys., 12, 4117–4125, doi:10.5194/acp-12-4117-2012, 2012.

Jokinen, T., Sipilä, M., Richters, S., Kerminen, V.-M., Paasonen, P., Stratmann, F., Worsnop, D., Kulmala, M., Ehn, M., Herrmann, H., and Berndt, T.: Rapid autoxidation forms highly oxidized RO_2 radicals in the atmosphere, Angew. Chem. Int. Edit., 53, 14596–14600, doi:10.1002/anie.201408566, 2014.

Junninen, H., Ehn, M., Petäjä, T., Luosujärvi, L., Kotiaho, T., Kostiainen, R., Rohner, U., Gonin, M., Fuhrer, K., Kulmala, M., and Worsnop, D. R.: A high-resolution mass spectrometer to measure atmospheric ion composition, Atmos. Meas. Tech., 3, 1039–1053, doi:10.5194/amt-3-1039-2010, 2010.

Formation of highly oxidized multifunctional compounds

T. F. Mentel et al.

Title Page

Abstract	Introduction
Conclusions	References
Tables	Figures

|◄ | ►|
◄ | ►

Back | Close

Full Screen / Esc

Printer-friendly Version

Interactive Discussion

Kerminen, V. M., Lihavainen, H., Komppula, M., Viisanen, Y., and Kulmala, M.: Direct observational evidence linking atmospheric aerosol formation and cloud droplet activation, Geophys. Res. Lett., 32, L14803, doi:10.1029/2005GL023130, 2005.

Kerminen, V.-M., Petäjä, T., Manninen, H. E., Paasonen, P., Nieminen, T., Sipilä, M., Junninen, H., Ehn, M., Gagné, S., Laakso, L., Riipinen, I., Vehkamäki, H., Kurten, T., Ortega, I. K., Dal Maso, M., Brus, D., Hyvärinen, A., Lihavainen, H., Leppä, J., Lehtinen, K. E. J., Mirme, A., Mirme, S., Hõrrak, U., Berndt, T., Stratmann, F., Birmili, W., Wiedensohler, A., Metzger, A., Dommen, J., Baltensperger, U., Kiendler-Scharr, A., Mentel, T. F., Wildt, J., Winkler, P. M., Wagner, P. E., Petzold, A., Minikin, A., Plass-Dülmer, C., Pöschl, U., Laaksonen, A., and Kulmala, M.: Atmospheric nucleation: highlights of the EUCAARI project and future directions, Atmos. Chem. Phys., 10, 10829–10848, doi:10.5194/acp-10-10829-2010, 2010.

Kirkby, J., Curtius, J., Almeida, J., Dunne, E., Duplissy, J., Ehrhart, S., Franchin, A., Gagne, S., Ickes, L., Kurten, A., Kupc, A., Metzger, A., Riccobono, F., Rondo, L., Schobesberger, S., Tsagkogeorgas, G., Wimmer, D., Amorim, A., Bianchi, F., Breitenlechner, M., David, A., Dommen, J., Downard, A., Ehn, M., Flagan, R. C., Haider, S., Hansel, A., Hauser, D., Jud, W., Junninen, H., Kreissl, F., Kvashin, A., Laaksonen, A., Lehtipalo, K., Lima, J., Lovejoy, E. R., Makhmutov, V., Mathot, S., Mikkila, J., Minginette, P., Mogo, S., Nieminen, T., Onnela, A., Pereira, P., Petaja, T., Schnitzhofer, R., Seinfeld, J. H., Sipilä, M., Stozhkov, Y., Stratmann, F., Tome, A., Vanhanen, J., Viisanen, Y., Vrtala, A., Wagner, P. E., Walther, H., Weingartner, E., Wex, H., Winkler, P. M., Carslaw, K. S., Worsnop, D. R., Baltensperger, U., and Kulmala, M.: Role of sulphuric acid, ammonia and galactic cosmic rays in atmospheric aerosol nucleation, Nature, 476, 429–433, doi:10.1038/nature10343, 2011.

Koop, T., Bookhold, J., Shiraiwa, M., and Poeschl, U.: Glass transition and phase state of organic compounds: dependency on molecular properties and implications for secondary organic aerosols in the atmosphere, Phys. Chem. Chem. Phys., 13, 19238–19255, doi:10.1039/c1cp22617g, 2011.

Kuang, C., McMurry, P. H., McCormick, A. V., and Eisele, F. L.: Dependence of nucleation rates on sulfuric acid vapor concentration in diverse atmospheric locations, J. Geophys. Res.-Atmos., 113, D10209, doi:10.1029/2007jd009253, 2008.

Kuang, C., McMurry, P. H., and McCormick, A. V.: Determination of cloud condensation nuclei production from measured new particle formation events, Geophys. Res. Lett., 36, L09822, doi:10.1029/2009gl037584, 2009.

Title Page

Abstract | Introduction

Conclusions | References

Tables | Figures

◀ | ▶

Back | Close

Full Screen / Esc

Printer-friendly Version

Interactive Discussion

Kulmala, M., Kerminen, V. M., Anttila, T., Laaksonen, A., and O'Dowd, C. D.: Organic aerosol formation via sulphate cluster activation, J. Geophys. Res.-Atmos., 109, D04205, doi:10.1029/2003jd003961, 2004a.

Kulmala, M., Vehkamaki, H., Petajda, T., Dal Maso, M., Lauri, A., Kerminen, V. M., Birmili, W., and McMurry, P. H.: Formation and growth rates of ultrafine atmospheric particles: a review of observations, J. Aerosol Sci., 35, 143–176, 2004b.

Kulmala, M., Kontkanen, J., Junninen, H., Lehtipalo, K., Manninen, H. E., Nieminen, T., Petaja, T., Sipilä, M., Schobesberger, S., Rantala, P., Franchin, A., Jokinen, T., Jarvinen, E., Aijala, M., Kangasluoma, J., Hakala, J., Aalto, P. P., Paasonen, P., Mikkila, J., Vanhanen, J., Aalto, J., Hakola, H., Makkonen, U., Ruuskanen, T., Mauldin, R. L., Duplissy, J., Vehkamaki, H., Back, J., Kortelainen, A., Riipinen, I., Kurten, T., Johnston, M. V., Smith, J. N., Ehn, M., Mentel, T. F., Lehtinen, K. E. J., Laaksonen, A., Kerminen, V. M., and Worsnop, D. R.: Direct observations of atmospheric aerosol nucleation, Science, 339, 943–946, doi:10.1126/science.1227385, 2013.

Mentel, Th. F., Wildt, J., Kiendler-Scharr, A., Kleist, E., Tillmann, R., Dal Maso, M., Fisseha, R., Hohaus, Th., Spahn, H., Uerlings, R., Wegener, R., Griffiths, P. T., Dinar, E., Rudich, Y., and Wahner, A.: Photochemical production of aerosols from real plant emissions, Atmos. Chem. Phys., 9, 4387–4406, doi:10.5194/acp-9-4387-2009, 2009.

Metzger, A., Verheggen, B., Dommen, J., Duplissy, J., Prevot, A. S. H., Weingartner, E., Riipinen, I., Kulmala, M., Spracklen, D. V., Carslaw, K. S., and Baltensperger, U.: Evidence for the role of organics in aerosol particle formation under atmospheric conditions, P. Natl. Acad. Sci. USA, 107, 6646–6651, doi:10.1073/pnas.0911330107, 2010.

Murphy, B. N., Donahue, N. M., Robinson, A. L., and Pandis, S. N.: A naming convention for atmospheric organic aerosol, Atmos. Chem. Phys., 14, 5825–5839, doi:10.5194/acp-14-5825-2014, 2014.

Nguyen, T. L., Vereecken, L., and Peeters, J.: HO$_x$ regeneration in the oxidation of isoprene III: theoretical study of the key isomerisation of the Z-delta-hydroxy-peroxy isoprene radicals, Chem. Phys. Chem., 11, 3996–4001, doi:10.1002/cphc.201000480, 2010.

Paasonen, P., Nieminen, T., Asmi, E., Manninen, H. E., Petäjä, T., Plass-Dülmer, C., Flentje, H., Birmili, W., Wiedensohler, A., Hõrrak, U., Metzger, A., Hamed, A., Laaksonen, A., Facchini, M. C., Kerminen, V.-M., and Kulmala, M.: On the roles of sulphuric acid and low-volatility organic vapours in the initial steps of atmospheric new particle formation, Atmos. Chem. Phys., 10, 11223–11242, doi:10.5194/acp-10-11223-2010, 2010.

Peeters, J., Nguyen, T. L., and Vereecken, L.: HO_x radical regeneration in the oxidation of isoprene, Phys. Chem. Chem. Phys., 11, 5935–5939, doi:10.1039/b908511d, 2009.

Riccobono, F., Rondo, L., Sipilä, M., Barmet, P., Curtius, J., Dommen, J., Ehn, M., Ehrhart, S., Kulmala, M., Kürten, A., Mikkilä, J., Paasonen, P., Petäjä, T., Weingartner, E., and Baltensperger, U.: Contribution of sulfuric acid and oxidized organic compounds to particle formation and growth, Atmos. Chem. Phys., 12, 9427–9439, doi:10.5194/acp-12-9427-2012, 2012.

Riccobono, F., Schobesberger, S., Scott, C. E., Dommen, J., Ortega, I. K., Rondo, L., Almeida, J., Amorim, A., Bianchi, F., Breitenlechner, M., David, A., Downard, A., Dunne, E. M., Duplissy, J., Ehrhart, S., Flagan, R. C., Franchin, A., Hansel, A., Junninen, H., Kajos, M., Keskinen, H., Kupc, A., Kuerten, A., Kvashin, A. N., Laaksonen, A., Lehtipalo, K., Makhmutov, V., Mathot, S., Nieminen, T., Onnela, A., Petaja, T., Praplan, A. P., Santos, F. D., Schallhart, S., Seinfeld, J. H., Sipilä, M., Spracklen, D. V., Stozhkov, Y., Stratmann, F., Tome, A., Tsagkogeorgas, G., Vaattovaara, P., Viisanen, Y., Vrtala, A., Wagner, P. E., Weingartner, E., Wex, H., Wimmer, D., Carslaw, K. S., Curtius, J., Donahue, N. M., Kirkby, J., Kulmala, M., Worsnop, D. R., and Baltensperger, U.: Oxidation products of biogenic emissions contribute to nucleation of atmospheric particles, Science, 344, 717–721, doi:10.1126/science.1243527, 2014.

Riipinen, I., Pierce, J. R., Yli-Juuti, T., Nieminen, T., Häkkinen, S., Ehn, M., Junninen, H., Lehtipalo, K., Petäjä, T., Slowik, J., Chang, R., Shantz, N. C., Abbatt, J., Leaitch, W. R., Kerminen, V.-M., Worsnop, D. R., Pandis, S. N., Donahue, N. M., and Kulmala, M.: Organic condensation: a vital link connecting aerosol formation to cloud condensation nuclei (CCN) concentrations, Atmos. Chem. Phys., 11, 3865–3878, doi:10.5194/acp-11-3865-2011, 2011.

Riipinen, I., Yli-Juuti, T., Pierce, J. R., Petaja, T., Worsnop, D. R., Kulmala, M., and Donahue, N. M.: The contribution of organics to atmospheric nanoparticle growth, Nat. Geosci., 5, 453–458, doi:10.1038/ngeo1499, 2012.

Rissanen, M. P., Kurteìn, T., Sipilä, M., Thornton, J. A., Kangasluoma, J., Sarnela, N., Junninen, H., Jørgensen, S., Schallhart, S., Kajos, M. K., Taipale, R., Springer, M., Mentel, T. F., Ruuskanen, T., Petäjä, T., Worsnop, D. R., Kjaergaard, H. G., and Ehn, M.: The formation of highly oxidized multifunctional products in the ozonolysis of cyclohexene, J. Am. Chem. Soc., 136, 15596–15606, doi:10.1021/ja507146s, 2014.

Schobesberger, S., Junninen, H., Bianchi, F., Lonn, G., Ehn, M., Lehtipalo, K., Dommen, J., Ehrhart, S., Ortega, I. K., Franchin, A., Nieminen, T., Riccobono, F., Hutterli, M., Du-

Title Page

Abstract | Introduction

Conclusions | References

Tables | Figures

|◀ | ▶|

◀ | ▶

Back | Close

Full Screen / Esc

Printer-friendly Version

Interactive Discussion

Discussion Paper | Discussion Paper | Discussion Paper | Discussion Paper

plissy, J., Almeida, J., Amorim, A., Breitenlechner, M., Downard, A. J., Dunne, E. M., Flagan, R. C., Kajos, M., Keskinen, H., Kirkby, J., Kupc, A., Kuerten, A., Kurten, T., Laaksonen, A., Mathot, S., Onnela, A., Praplan, A. P., Rondo, L., Santos, F. D., Schallhart, S., Schnitzhofer, R., Sipilä, M., Tome, A., Tsagkogeorgas, G., Vehkamaki, H., Wimmer, D., Baltensperger, U., Carslaw, K. S., Curtius, J., Hansel, A., Petaja, T., Kulmala, M., Donahue, N. M., and Worsnop, D. R.: Molecular understanding of atmospheric particle formation from sulfuric acid and large oxidized organic molecules, P. Natl. Acad. Sci. USA, 110, 17223–17228, doi:10.1073/pnas.1306973110, 2013.

Shiraiwa, M., Zuend, A., Bertram, A. K., and Seinfeld, J. H.: Gas-particle partitioning of atmospheric aerosols: interplay of physical state, non-ideal mixing and morphology, Phys. Chem. Chem. Phys., 15, 11441–11453, doi:10.1039/c3cp51595h, 2013.

Sipilä, M., Berndt, T., Petaja, T., Brus, D., Vanhanen, J., Stratmann, F., Patokoski, J., Mauldin, R. L., III, Hyvarinen, A.-P., Lihavainen, H., and Kulmala, M.: The role of sulfuric acid in atmospheric nucleation, Science, 327, 1243–1246, doi:10.1126/science.1180315, 2010.

Spracklen, D. V., Carslaw, K. S., Merikanto, J., Mann, G. W., Reddington, C. L., Pickering, S., Ogren, J. A., Andrews, E., Baltensperger, U., Weingartner, E., Boy, M., Kulmala, M., Laakso, L., Lihavainen, H., Kivekäs, N., Komppula, M., Mihalopoulos, N., Kouvarakis, G., Jennings, S. G., O'Dowd, C., Birmili, W., Wiedensohler, A., Weller, R., Gras, J., Laj, P., Sellegri, K., Bonn, B., Krejci, R., Laaksonen, A., Hamed, A., Minikin, A., Harrison, R. M., Talbot, R., and Sun, J.: Explaining global surface aerosol number concentrations in terms of primary emissions and particle formation, Atmos. Chem. Phys., 10, 4775–4793, doi:10.5194/acp-10-4775-2010, 2010.

Vereecken, L. and Francisco, J. S.: Theoretical studies of atmospheric reaction mechanisms in the troposphere, Chemical Soc. Rev., 41, 6259–6293, doi:10.1039/c2cs35070j, 2012.

Vereecken, L. and Peeters, J.: A structure–activity relationship for the rate coefficient of H-migration in substituted alkoxy radicals, Phys. Chem. Chem. Phys., 12, 12608–12620, doi:10.1039/c0cp00387e, 2010.

Vereecken, L., Mueller, J. F., and Peeters, J.: Low-volatility poly-oxygenates in the OH-initiated atmospheric oxidation of alpha-pinene: impact of non-traditional peroxyl radical chemistry, Phys. Chem. Chem. Phys., 9, 5241–5248, doi:10.1039/b708023a, 2007.

Virtanen, A., Joutsensaari, J., Koop, T., Kannosto, J., Yli-Pirila, P., Leskinen, J., Makela, J. M., Holopainen, J. K., Poeschl, U., Kulmala, M., Worsnop, D. R., and Laaksonen, A.: An amor-

Title Page

Abstract | Introduction

Conclusions | References

Tables | Figures

|◀ | ▶|

◀ | ▶

Back | Close

Full Screen / Esc

Printer-friendly Version

Interactive Discussion

phous solid state of biogenic secondary organic aerosol particles, Nature, 467, 824–827, doi:10.1038/nature09455, 2010.

Vuollekoski, H., Nieminen, T., Paasonen, P., Sihto, S.-L., Boy, M., Manninen, H., Lehtinen, K., Kerminen, V.-M., and Kulmala, M.: Atmospheric nucleation and initial steps of particle growth: numerical comparison of different theories and hypotheses, Atmos. Res., 98, 229–236, doi:10.1016/j.atmosres.2010.04.007, 2010.

Yli-Juuti, T., Nieminen, T., Hirsikko, A., Aalto, P. P., Asmi, E., Hõrrak, U., Manninen, H. E., Patokoski, J., Dal Maso, M., Petäjä, T., Rinne, J., Kulmala, M., and Riipinen, I.: Growth rates of nucleation mode particles in Hyytiälä during 2003–2009: variation with particle size, season, data analysis method and ambient conditions, Atmos. Chem. Phys., 11, 12865–12886, doi:10.5194/acp-11-12865-2011, 2011.

Zhang, R. Y., Suh, I., Zhao, J., Zhang, D., Fortner, E. C., Tie, X. X., Molina, L. T., and Molina, M. J.: Atmospheric new particle formation enhanced by organic acids, Science, 304, 1487–1490, doi:10.1126/science.1095139, 2004.

Zhao, J., Smith, J. N., Eisele, F. L., Chen, M., Kuang, C., and McMurry, P. H.: Observation of neutral sulfuric acid-amine containing clusters in laboratory and ambient measurements, Atmos. Chem. Phys., 11, 10823–10836, doi:10.5194/acp-11-10823-2011, 2011.

Zobrist, B., Marcolli, C., Pedernera, D. A., and Koop, T.: Do atmospheric aerosols form glasses? Atmos. Chem. Phys., 8, 5221–5244, 2008, http://www.atmos-chem-phys.net/8/5221/2008/.

Formation of highly oxidized multifunctional compounds

T. F. Mentel et al.

Title Page

Abstract	Introduction
Conclusions	References
Tables	Figures

Back | Close

Full Screen / Esc

Printer-friendly Version

Interactive Discussion

Table 1. VOC investigated in this study, steady state mixing ratio of VOC and O_3 during the ozonolysis experiments, rate coefficient for the VOC + O_3 reactions at 298 K.

VOC	Molecular formula	Molar mass [$\mathrm{g\,mol^{-1}}$]	Purity [%]	[VOC]$_{SS}$ [ppb]	[O_3]$_{SS}$ [ppb]	$k^5_{O_3+VOC}$ [$\mathrm{cm^3\,s^{-1}}$]
cyclopentene[2]	C_5H_8	68.12	96	81	90	6.5×10^{-16}
cyclohexene[1]	C_6H_{10}	82.14	> 99	136	65	8×10^{-17}
1-methyl-cyclohexene[1]	C_7H_{12}	96.17	97	50	75	1.5×10^{-16}
3-methyl-cyclohexene[2]	C_7H_{12}	96.17	> 93	26	84	5.5×10^{-17}
4-methyl-cyclohexene[2]	C_7H_{12}	96.17	98	88	70	7×10^{-17}
cycloheptene[1]	C_7H_{12}	96.16	97	40	80	2.5×10^{-16}
1-heptene[1]	C_7H_{14}	98.19	97	33	105	1.5×10^{-17}
(Z)-6-nonenal[1]	$C_9H_{16}O$	140.22	92	44	90	
(Z)-6-nonen-(1)-ol[3]	$C_9H_{18}O$	142.4	≥ 95	1.4	80	
5-hexen-2-one[1]	$C_6H_{10}O$	98.14	99	33	90	
α-pinene[1]	$C_{10}H_{16}$	136.24	> 99	10	100	9×10^{-17}
Δ-3-carene[4]	$C_{10}H_{16}$	136.24	≥ 98.5	10	100	4×10^{-17}

[1] Aldrich,
[2] TCI,
[3] SAFC,
[4] Fluka,
[5] NIST Gas Phase Kinetic Data Base (http://kinetics.nist.gov/kinetics/).

Table 2. a) Possible peroxy radicals from cyclopentene and products of their reactions with peroxy radicals (cf. Sequence 2). b) Analogous scheme for the hydroxy-peroxy path. The first peroxy radical in Table 2b arise from the first peroxy radical in Table 2a by reaction with another peroxy radical (or NO).

	Peroxy radical	Carbonyl	Hydroxy	Hydroperoxy
A	m	$m-17$	$m-15$	$m+1$
autoxidation	$C_5H_7O_4$ 131 Da	$C_5H_6O_3$ 114 Da	$C_5H_8O_3$ 116 Da	$C_5H_8O_4$ 132 Da
↓	$C_5H_7O_6$ 163 Da	$C_5H_6O_5$ 146 Da	$C_5H_8O_5$ 148 Da	$C_5H_8O_6$ 164 Da
	$C_5H_7O_8$ 195 Da	$C_5H_6O_7$ 178 Da	$C_5H_8O_7$ 180 Da	$C_5H_8O_8$ 196 Da
	$C_5H_7O_{10}$ 227 Da	$C_5H_6O_9$ 210 Da	$C_5H_8O_9$ 212 Da	$C_5H_8O_{10}$ 228 Da
		termination →		
B	m	$m-17$	$m-15$	$m+1$
autoxidation after Sequence 3	$C_5H_7O_5$ 147 Da	$C_5H_6O_4$ 130 Da	$C_5H_8O_4$ 132 Da	$C_5H_8O_5$ 148 Da
↓	$C_5H_7O_7$ 179 Da	$C_5H_6O_6$ 162 Da	$C_5H_8O_6$ 164 Da	$C_5H_8O_7$ 180 Da
	$C_5H_7O_9$ 211 Da	$C_5H_6O_8$ 194 Da	$C_5H_8O_8$ 196 Da	$C_5H_8O_9$ 212 Da
		termination →		

Table 3. Observation of HOM formation as function of compound and functionalization

Compound	Formula	HOM products	ω-Terminal group[*]
Cyclic alkenes			
cyclopentene	C_5H_8	yes	aldehyde
cyclohexene	C_6H_{10}	yes	aldehyde
cycloheptene	C_7H_{12}	yes	aldehyde
1-methyl-cyclohexene	C_7H_{12}	yes	ketone/aldehyde
3-methyl-cyclohexene	C_7H_{12}	yes	aldehyde
4-methyl-cylohexene	C_7H_{12}	yes	aldehyde
Linear alkene			
1-heptene	C_7H_{14}	no	methyl
Linear alkenes with additional functional group			
(Z)-6-nonenal	$C_9H_{16}O$	yes	aldehyde
(Z)-6-nonenol	$C_9H_{17}OH$	no	alcohol
5-hexen-2-on	$C_6H_{10}O$	no	ketone
Monoterpenes			
α-pinene	$C_{10}H_{16}$	yes	ketone/aldehyde
Δ-3-carene	$C_{10}H_{16}$	yes	ketone/aldehyde

[*] at the opposite end to the oxoic radical groups in Fig. 3.

Table 4. HOM observed during ozonolysis of cyclopentene. The second header line shows at which molar masses the termination products are expected relative to the peroxy radical with molar mass m (unit masses). Filled cells indicate that these compounds were detected with given elemental composition and relative intensity (second line in the same cell). Relative intensities were normalized to the largest HOM signal. The third line in the cell gives the molar mass [Da] in unit mass resolution and the precise m/z [Th] at which the molecule was detected as cluster with $^{15}NO_3^-$.

Peroxy radical	Carbonyl	Hydroxy	Hydroperoxy
m	$m-17$	$m-15$	$m+1$
$C_5H_7O_8$ 54 % 195/257.9995	$C_5H_6O_7$ 100 % 178/240.996	$C_5H_8O_7$ 14 % 180/243.0124	$C_5H_8O_8$ 19 %[2] 196/259.0073
$C_5H_7O_9^1$ 1 % 211/273.9944		$C_5H_8O_8$ 19 %[2] 196/259.0073	
$C_5H_7O_{10}$ 6 % 227/289.9893	$C_5H_6O_9$ 43 % 210/272.9866	$C_5H_8O_9$ 11 % 212/275.0022	

[1] hydroxy-peroxy path Sequence 3.
[2] $C_5H_7O_8 + HO_2 \rightarrow C_5H_8O_8$ or $C_5H_7O_9 + RO_2 \rightarrow C_5H_8O_8$.

Full Screen / Esc

Table 5. HOM observed during ozonolysis of cyclohexene. The second header line shows at which molar masses the termination products are expected relative to the peroxy radical with molar mass m (unit masses). Filled cells indicate that these compounds were detected with given elemental composition and relative intensity (second line in the same cell). Relative intensities were normalized to the largest HOM signal. The third line in the cell gives the molar mass [Da] in unit mass resolution and the precise m/z [Th] at which the molecule was detected as cluster with $^{15}NO_3^-$.

Peroxy radical	Carbonyl	Hydroxy	Hydroperoxy
m	$m-17$	$m-15$	$m+1$
$C_6H_9O_8$ 7 % 209/272.01453	$C_6H_8O_7$ 24 % 192/255.01270	$C_6H_{10}O_7$ 1 % 194/257.02523	$C_6H_{10}O_8$ 5 % 210/273.0230
	$C_6H_8O_8{}^*$ 14 % 208/271.00724		
$C_6H_9O_{10}$ < 1 % 241/304.00582	$C_6H_8O_9$ 100 % 224/287.0024		$C_6H_{10}O_{10}$ < 1 % 242/305.00889

* hydroxy-peroxy path Sequence 3.

Table 6. HOM observed during ozonolysis of cycloheptene. The second header line shows at which molar masses the termination products are expected relative to the peroxy radical with molar mass m (unit masses). Filled cells indicate that these compounds were detected with given elemental composition and relative intensity (second line in the same cell). Relative intensities were normalized to the largest HOM signal. The third line in the cell gives the molar mass [Da] in unit mass resolution and the precise m/z [Th] at which the molecule was detected as cluster with $^{15}NO_3^-$.

Peroxy radical	Carbonyl	Hydroxy	Hydroperoxy
m	$m-17$	$m-15$	$m+1$
	$C_7H_{10}O_5$ < 1 % 174/237.0395		
$C_7H_{11}O_7^*$ < 1 % 206/269.0462			
$C_7H_{11}O_8$ 2 % 223/286.02945	$C_7H_{10}O_7$ 3 % 206/269.02775	$C_7H_{12}O_7$ < 1 % 208/271.0409	
	$C_7H_{10}O_8^*$ 8 % 222/285.02306		
$C_7H_{11}O_{10}$ 1 % 255/318.02027	$C_7H_{10}O_9$ 100 % 238/301.01758		$C_7H_{12}O_{10}$ < 1 % 256/319.02544
$C_7H_{11}O_{11}^*$ < 1 % 271/334.01508	$C_7H_{10}O_{10}^*$ < 1 % 254/317.0141		

* hydroxy-peroxy path Sequence 3.

Formation of highly oxidized multifunctional compounds

T. F. Mentel et al.

Table 7. HOM observed during ozonolysis of (Z)-6-nonenal. The second header line shows at which molar masses the termination products are expected relative to the peroxy radical with molar mass m (unit masses). Filled cells indicate that these compounds were detected with given elemental composition and relative intensity (second line in the same cell). Relative intensities were normalized to the largest HOM signal. The third line in the cell gives the molar mass [Da] in unit mass resolution and the precise m/z [Th] at which the molecule was detected as cluster with $^{15}NO_3^-$.

Peroxy radical	Carbonyl	Hxdroxy	Hydroperoxy
m	$m-17$	$m-15$	$m+1$
$C_6H_9O_8$ 10 % 209/272.0151			
$C_6H_9O_9$* 3 % 225/288.0101			
$C_6H_8O_{10}$ 5 % 241/304.0050	$C_6H_8O_9$ 100 % 224/287.0022		

* hydroxy-peroxy path sequence 3.

Table 8. HOM observed during ozonolysis of 1-methylcyclohexene. The second header line shows at which molar masses the termination products are expected relative to the peroxy radical with molar mass m (unit masses). Filled cells indicate that these compounds were detected with given elemental composition and relative intensity (second line in the same cell). Relative intensities were normalized to the largest HOM signal. The third line in the cell gives the molar mass [Da] in unit mass resolution and the precise m/z [Th] at which the molecule was detected as cluster with $^{15}NO_3^-$.

Peroxy radical	Carbonyl	Hydroxy	Hydroperoxy
m	$m-17$	$m-15$	$m+1$
$C_7H_{11}O_6$ < 1 % 191/254.03857	$C_7H_{10}O_5$ < 1 % 174/237.03855		
$C_7H_{11}O_7^*$ < 1 % 207/270.03179	$C_7H_{10}O_6^*$ 1 % 190/253.0331		
$C_7H_{11}O_8$ 2 % 223/286.03086	$C_7H_{10}O_7$ 100 % 206/269.02829	$C_7H_{12}O_7$ 2 % 208/271.3858	$C_7H_{12}O_8$ 1 % 224/287.04046
$C_7H_{11}O_9^*$ < 1 % 239/302.02700			
	$C_7H_{10}O_9$ < 1 % 238/301.01326	$C_7H_{12}O_9$ < 1 % 240/303.03521	

* hydroxy-peroxy path sequence 3.

Table 9. HOM products observed during ozonolysis of 3-methylcyclohexene. The second header line shows at which molar masses the termination products are expected relative to the peroxy radical with molar mass m (unit masses). Filled cells indicate that these compounds were detected with given elemental composition and relative intensity (second line in the same cell). Relative intensities were normalized to the largest HOM signal. The third line in the cell gives the molar mass [Da] in unit mass resolution and the precise m/z [Th] at which the molecule was detected as cluster with $^{15}NO_3^-$.

Peroxy radical	Carbonyl	Hydroxy	Hydroperoxy
m	$m-17$	$m-15$	$m+1$
	$C_7H_{10}O_5$ $< 1\%$ 174/237.0382		
	$C_7H_{10}O_6{}^*$ $< 1\%$ 190/253.0331		
$C_7H_{11}O_8$ 12% 223/286.0308	$C_7H_{10}O_7$ 25% 206/269.0281		$C_7H_{12}O_8$ 6% 224/287.0386
$C_7H_{11}O_9{}^*$ 5% 239/302.0257	$C_7H_{10}O_8{}^*$ 19% 222/285.0230		
$C_7H_{11}O_{10}$ 9% 255/318.0206	$C_7H_{10}O_9$ 100% 238/301.0179	$C_7H_{12}O_9$ 13% 240/303.0335	

[*] hydroxy-peroxy path sequence 3.

Formation of highly oxidized multifunctional compounds

T. F. Mentel et al.

Discussion Paper | Discussion Paper | Discussion Paper | Discussion Paper | Discussion Paper

Table 10. HOM products observed during ozonolysis of 4-methyl-cyclohexene. The second header line shows at which molar masses the termination products are expected relative to the peroxy radical with molar mass m (unit masses). Filled cells indicate that these compounds were detected with given elemental composition and relative intensity (second line in the same cell). Relative intensities were normalized to the largest HOM signal. The third line in the cell gives the molar mass [Da] in unit mass resolution and the precise m/z [Th] at which the molecule was detected as cluster with $^{15}NO_3^-$.

Peroxy radical	Carbonyl	Hydroxy	Hydroperoxy
m	$m-17$	$m-15$	$m+1$
	$C_7H_{10}O_5$ < 1 % 174/237.03635		
$C_7H_{11}O_7{}^*$ < 1 % 207/270.0359	$C_7H_{10}O_6{}^*$ < 1 % 190/253.03390		
$C_7H_{11}O_8$ < 1 % 223/286.02825	$C_7H_{10}O_7$ 2 % 206/269.0281	$C_7H_{12}O_7$ < 1 % 208/271.0437	$C_7H_{12}O_8$ < 1 % 224/287.03770
$C_7H_{11}O_9{}^*$ < 1 % 239/302.0224	$C_7H_{10}O_8{}^*$ 5 % 222/285.02215		
$C_7H_{11}O_{10}$ 2 % 255/318.02114	$C_7H_{10}O_9$ 100 % 238/301.01848		$C_7H_{12}O_{10}$ < 1 % 256/319.02566
$C_7H_{11}O_{11}{}^*$ < 1 % 271/334.01626	$C_7H_{10}O_{10}{}^*$ 1 % 254/317.01331		
	$C_7H_{10}O_{11}$ < 1 % 270/333.01163	$C_7H_{12}O_{11}$ < 1 % 272/335.02524	

* hydroxy-peroxy path sequence 3.

Title Page

Abstract | Introduction

Conclusions | References

Tables | Figures

|◄ | ►|

◄ | ►

Back | Close

Full Screen / Esc

Printer-friendly Version

Interactive Discussion

Table 11. Comparison of HOM products resulting from C_7H_{14} compounds.

	Cycloheptene	1-MCH	3-MCH	4-MCH
Peroxy radical				
$C_7H_{11}O_6$	–	X	–	–
$C_7H_{11}O_8$	X	X	X	X
$C_7H_{11}O_{10}$	X	–	X	X
Carbonyl				
$C_7H_{10}O_5$	X	X	X	X
$C_7H_{10}O_7$	X	X	X	X
$C_7H_{10}O_9$	X	X	X	X
$C_7H_{10}O_{11}$	–	–	–	X
Hydroxy				
$C_7H_{12}O_7$	X	X	–	X
$C_7H_{12}O_9$	–	X	X	–
$C_7H_{12}O_{11}$	–	–	–	X
Hydroperoxy				
$C_7H_{12}O_6$	–	interference	–	–
$C_7H_{12}O_8$	–	X	X	X
$C_7H_{12}O_{10}$	X	–	–	X
Hydroxy-peroxy radical				
$C_7H_{11}O_7$	X	X	–	X
$C_7H_{11}O_9$	–	X	X	X
$C_7H_{11}O_{11}$	X	–	–	X
Hydroxy-peroxy path carbonyl				
$C_7H_{10}O_6$	–	X	X	X
$C_7H_{10}O_8$	X	–	X	X
$C_7H_{10}O_{10}$	X	–	–	X

Table 12. HOM products observed during ozonolysis of α-pinene. The second header line shows at which molar masses the termination products are expected relative to the peroxy radical with molar mass m (unit masses). Filled cells indicate that these compounds were detected with given elemental composition and relative intensity (second line in the same cell). Relative intensities were normalized to the largest HOM signal. The third line in the cell gives the molar mass [Da] in unit mass resolution and the precise m/z [Th] at which the molecule was detected as cluster with $^{15}NO_3^-$.

Peroxy radical	Carbonyl	Hydroxy	Hydroperoxy
m	$m-17$	$m-15$	$m+1$
$C_{10}H_{15}O_8$ 46 % 263/326.0621	$C_{10}H_{14}O_7$ 88 % 264/309.0594		
$C_{10}H_{15}O_9{}^*$ 5 % 279/342.0570	$C_{10}H_{14}O_8{}^*$ 14 % 262/325.0543		
$C_{10}H_{15}O_{10}$ 40 % 295/358.0519	$C_{10}H_{14}O_9$ 83 % 326/341.0492	$C_{10}H_{16}O_9$ 100 % 280/343.0648	$C_{10}H_{16}O_{10}$ 37 % 296/359.0597
	$C_{10}H_{14}O_{11}{}^*$ 69 % 327/373.0390	$C_{10}H_{16}O_{11}{}^*$ 29 % 312/375.0547	

* hydroxy-peroxy path sequence 3.

Table 13. HOM products observed during ozonolysis of Δ-3-carene. The second header line shows at which molar masses the termination products are expected relative to the peroxy radical with molar mass m (unit masses). Filled cells indicate that these compounds were detected with given elemental composition and relative intensity (second line in the same cell). Relative intensities were normalized to the largest HOM signal. The third line in the cell gives the molar mass [Da] in unit mass resolution and the precise m/z [Th] at which the molecule was detected as cluster with $^{15}NO_3^-$.

Peroxy radical	Carbonyl	Hydroxy	Hydroperoxy
m	$m-17$	$m-15$	$m+1$
$C_{10}H_{15}O_8$ 10 % 263/326.0621			
$C_{10}H_{15}O_{10}$ 94 % 295/358.0519	$C_{10}H_{14}O_9$ 47 % 278/341.0492	$C_{10}H_{16}O_9$ 100 % 280/343.0648	

Table 14. Detected and identified dimers observed during ozonolysis of cyclopentene.

m/z [Th]	Formula	Intensity [%]
389.0339	$C_{10}H_{14}O_{12} \cdot {}^{15}NO_3^-$	44
421.0238	$C_{10}H_{14}O_{14} \cdot {}^{15}NO_3^-$	100
453.0136	$C_{10}H_{14}O_{16} \cdot {}^{15}NO_3^-$	2
343.0648	$C_{10}H_{16}O_9 \cdot {}^{15}NO_3^-$	24
375.0547	$C_{10}H_{16}O_{11} \cdot {}^{15}NO_3^-$	6

Table 15. Possible dimers produced by permutations reactions of the monomer peroxy radicals of cyclopentene. Bold font: entities were detected. Italic font: dimers were detected and arise from two most abundant peroxy radicals.

	$C_5H_7O_6$	$C_5H_7O_7$	$\mathbf{C_5H_7O_8}$	$C_5H_7O_9$	$\mathbf{C_5H_7O_{10}}$
$C_5H_7O_6$	$C_{10}H_{14}O_{10}$	$C_{10}H_{14}O_{11}$	$\mathbf{C_{10}H_{14}O_{12}}$	$C_{10}H_{14}O_{13}$	$\mathbf{C_{10}H_{14}O_{14}}$
$C_5H_7O_7$		$\mathbf{C_{10}H_{14}O_{12}}$	$C_{10}H_{14}O_{13}$	$\mathbf{C_{10}H_{14}O_{14}}$	$C_{10}H_{14}O_{15}$
$\mathbf{C_5H_7O_8}$			$\mathit{C_{10}H_{14}O_{14}}$	$C_{10}H_{14}O_{15}$	$\mathit{C_{10}H_{14}O_{16}}$
$\mathbf{C_5H_7O_9}$				$\mathbf{C_{10}H_{14}O_{16}}$	$C_{10}H_{14}O_{17}$
$\mathbf{C_5H_7O_{10}}$					$C_{10}H_{14}O_{18}$
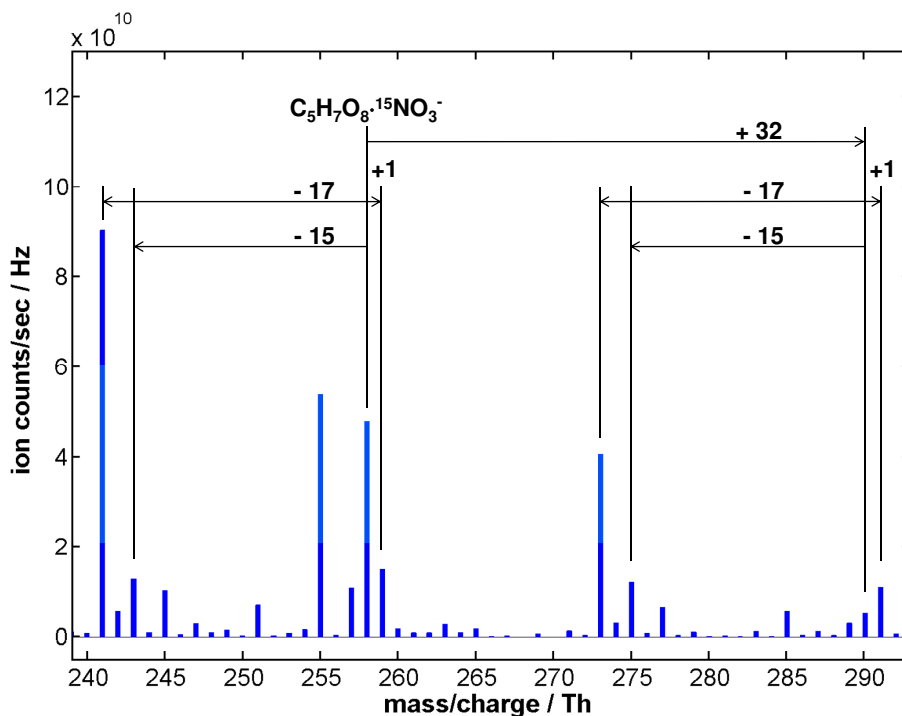
Figure 1. Spectrum of ozonolysis products of cyclopentene. The most abundant peroxy radical $C_5H_7O_8 \cdot {}^{15}NO_3^-$ and its termination products are marked as well as the next higher peroxy radical (+32 Th) and termination products. The m/z differences in [Th] are indicated.

Title Page

Abstract | Introduction

Conclusions | References

Tables | Figures

|◄ | ►|

◄ | ►

Back | Close

Full Screen / Esc

Printer-friendly Version

Interactive Discussion
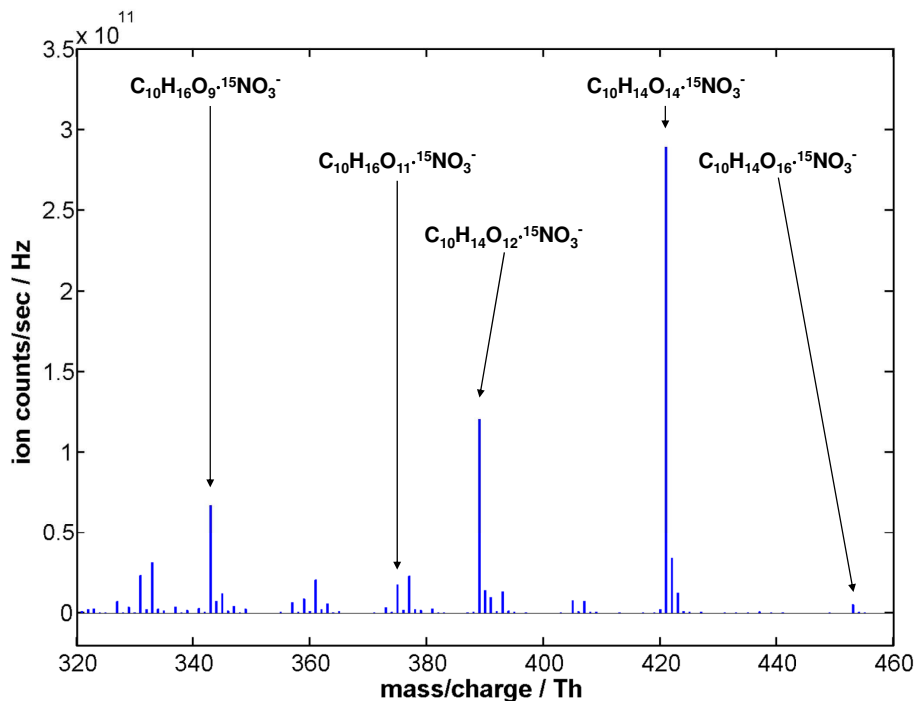
Figure 2. Spectrum of ozonolysis products of cyclopentene with dimer character. The detected elemental compositions are indicated (cf. Sect. 5.4).

Title Page

Abstract | Introduction

Conclusions | References

Tables | Figures

|◄ | ►|

◄ | ►

Back | Close

Full Screen / Esc
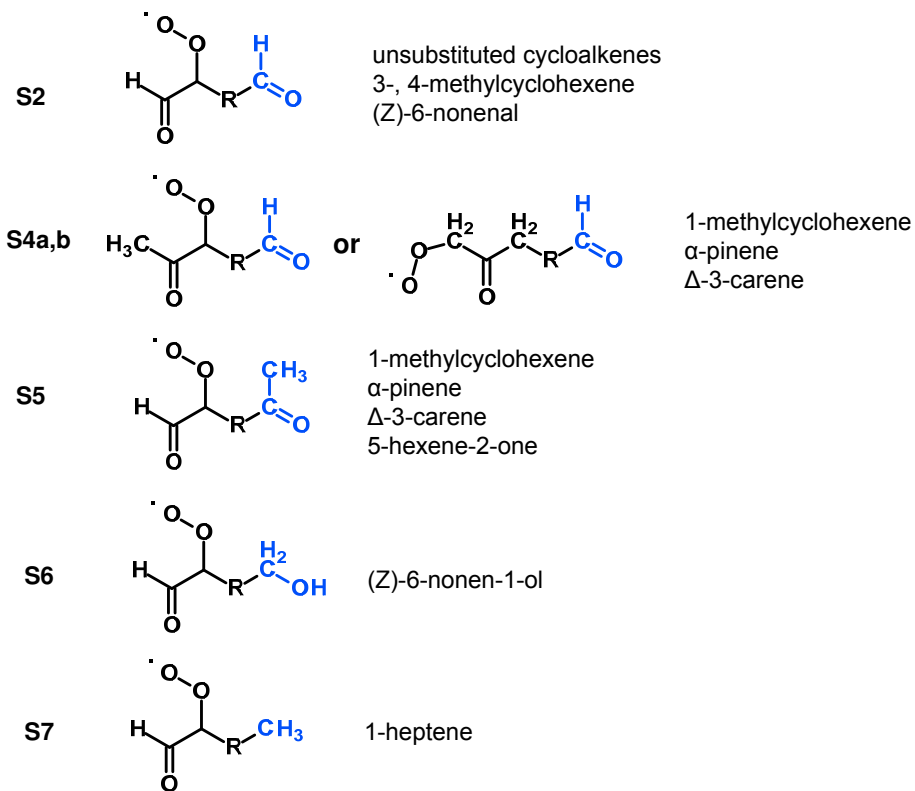
Figure 3. Peroxy radicals of the investigated VOC as expected from the vinylhydroperoxide path. Position of the peroxy group and functionality at the ϖ-terminal end.
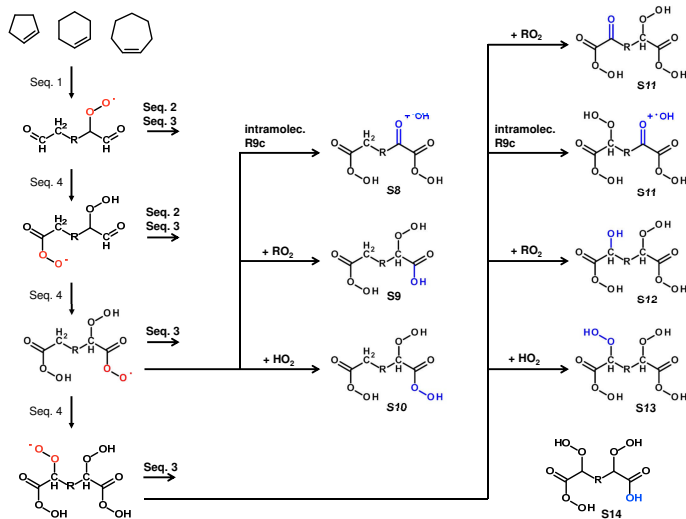
Figure 4. Examplaric mechanistic scheme in accordance with the results of the ozonolysis of cycloalkenes. Cyclopentene: $R = (CH_2)$, cyclohexene: $R = (CH_2)_2$, cycloheptene: $R = (CH_2)_3$. The peroxy radicals with increasing number of O-atoms ($m/z = m$) on the left hand side are formed by autoxidation (Sequence 4). They can undergo either termination reactions in Sequence 2 or follow the hydroxy-peroxy path (Sequence 3). The carbonyl ($m - 17$), hydroxy ($m - 15$) and hydroperoxy ($m + 1$) termination products are shown for the O_8-peroxy radical (S8–S10) and the O_{10}-peroxy radical (S11–S12) in the middle and right hand column, respectively. The functional groups formed by the termination reactions are shown in blue. The products S8 and S11 from the intramolecular termination R9c are the same as for the intermolecular termination reactions R5a and R6b. Note that in principle the series of rearrangements can be also permuted. If the H-atoms at the C-atom in α-position to the second aldehyde group are subject to H-shift before attack on the aldehyde group itself, structures like S14 could be formed, isobaric to S12.
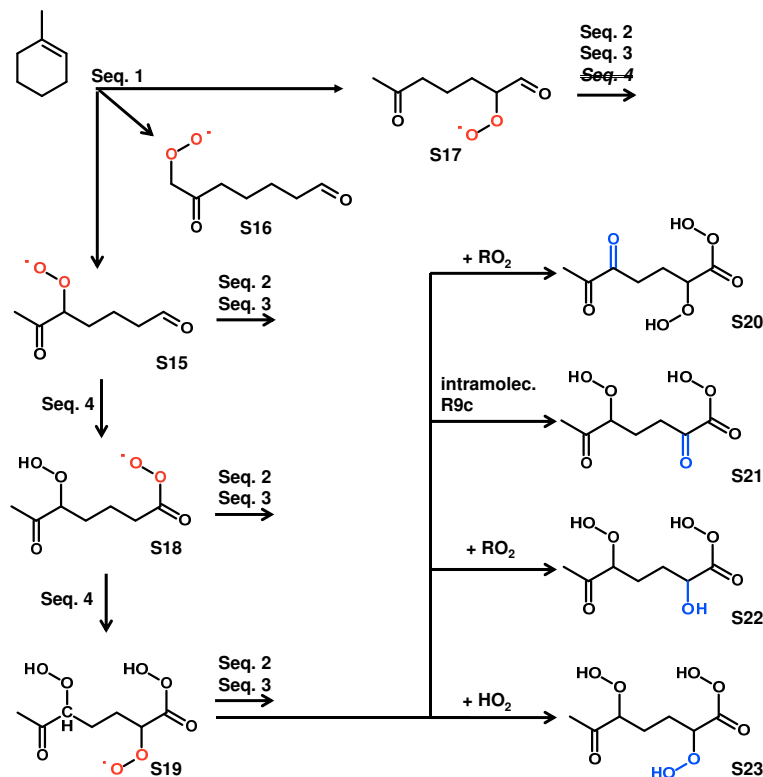
Figure 5. Schematics of HOM formation of 1-methyl cyclohexene. The major products are carbonyl termination products, either S20 or S21. Higher oxidation products are minor. Peroxy radical S17 has no terminal ω-aldehyde group. Peroxy radical S16 will produce isobaric products analogous to S15.
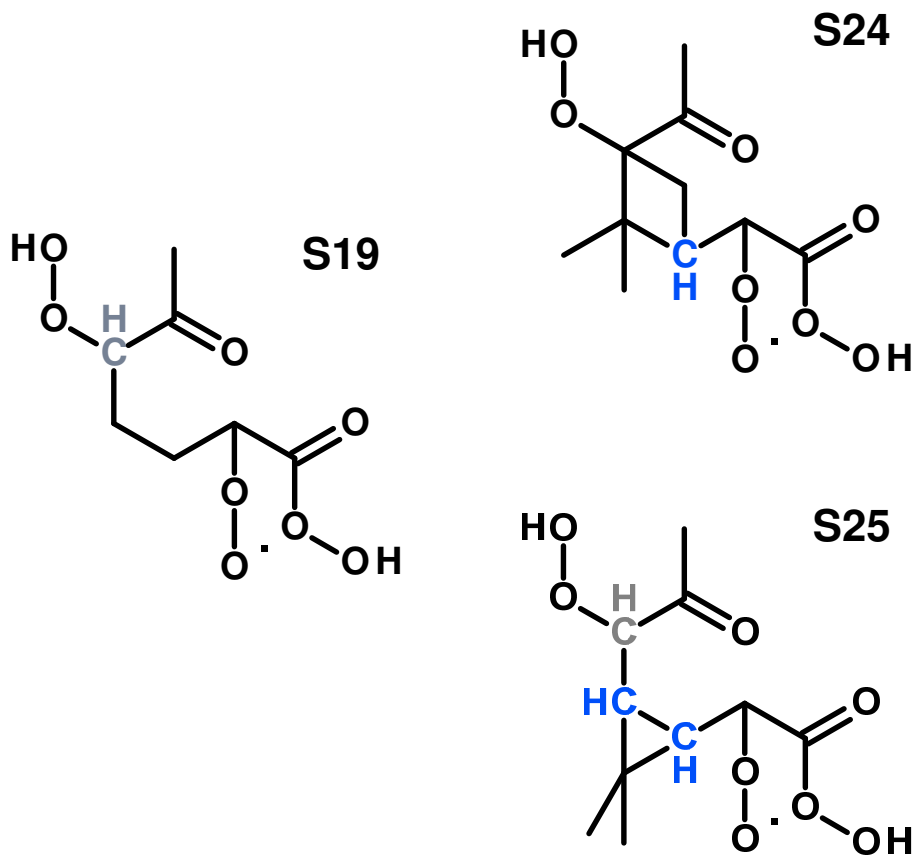
Figure 6. Comparison of *deduced* highest oxidized O_8-peroxy radical of 1-methyl cyclohexene (S19) to analogously *constructed* O_8-peroxy radicals of α-pinene (S24) and Δ-3-carene (S25). Tertiary H-atoms in blue are explicitely shown. The H at the carbon atom carrying the hydroperoxy group, which is shifted in R9c is shown in grey. In an isomeric modification the hydroperoxide group at C_3 could be located also at C_1.

Title Page

Abstract | Introduction

Conclusions | References

Tables | Figures

|◄ | ►|

◄ | ►

Back | Close

Full Screen / Esc
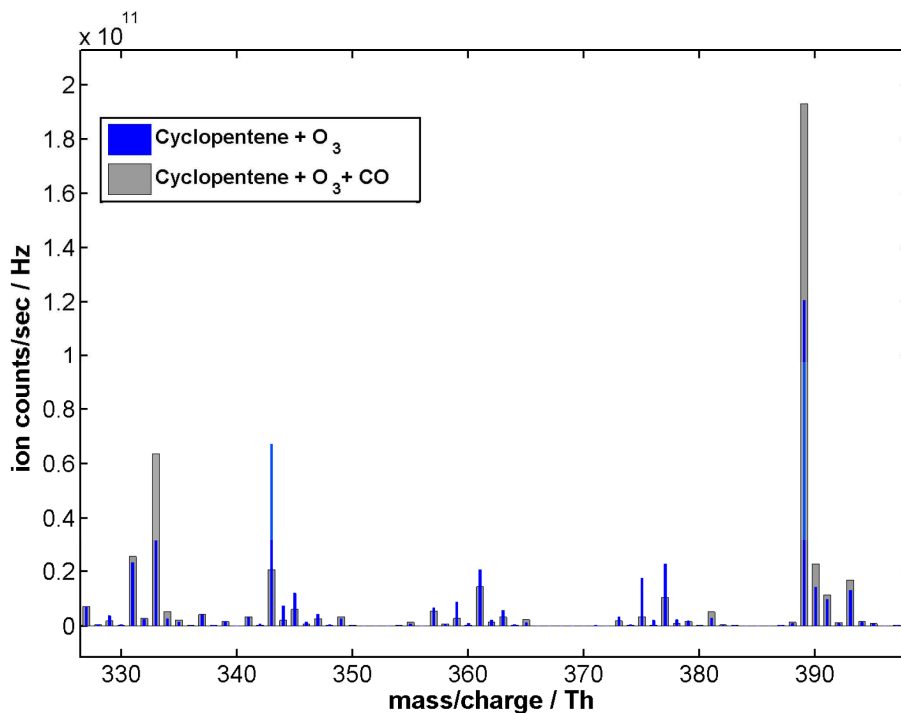
Figure 7. Comparison of the dimer HOM spectra resulting from ozonolysis of cyclopentene with CO addition (grey) and without CO addition (blue). The fraction of dimers which involve the O_3-peroxy radical from the addition of OH to the double bond of cyclopentene are reduced.
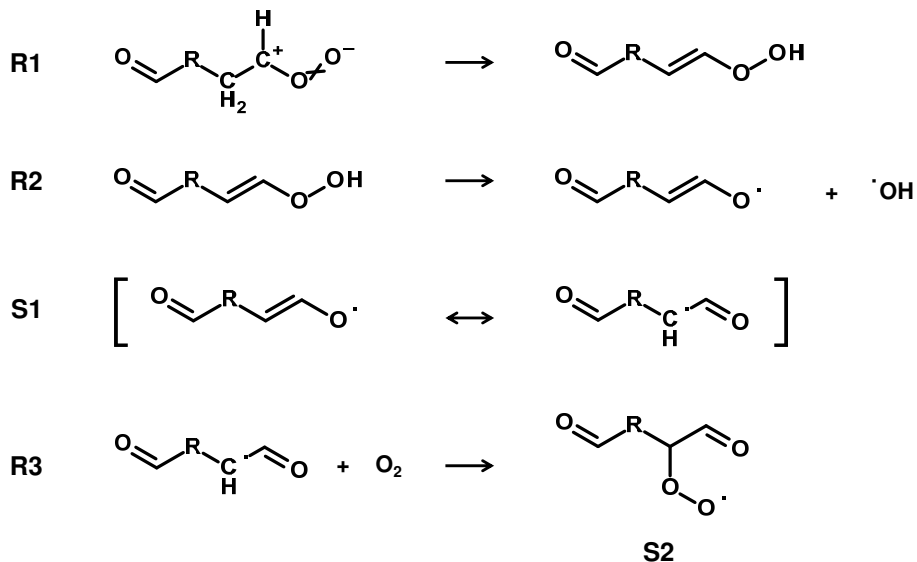
Sequence 1. Vinylhydroperoxide path in ozonolysis.

R4   hydroperoxy channel: $RO_2 + HO_2 \rightarrow ROOH + O_2$

R5a carbonyl channel: $RO_2 + R'O_2 \rightarrow R{=}O \quad + R'{\text{-}}OH + O_2$

R5b hydroxy channel: $RO_2 + R'O_2 \rightarrow ROH \quad + R'{=}O \;+ O_2$

R6a alkoxy channel: $RO_2 + R'O_2 \rightarrow RO \quad\; + O_2 \quad\; + products$

R6b alkoxy termination: $RO + O_2 \rightarrow R{=}O \quad + HO_2$

R7a NO alkoxy channel: $RO_2 + NO \rightarrow RO \quad\; + NO_2$

R7b NO org. nitrate channel: $RO_2 + NO \rightarrow RONO_2$

R8   peroxide channel (dimeriz.): $RO_2 + R'O_2 \rightarrow ROOR' + O_2$
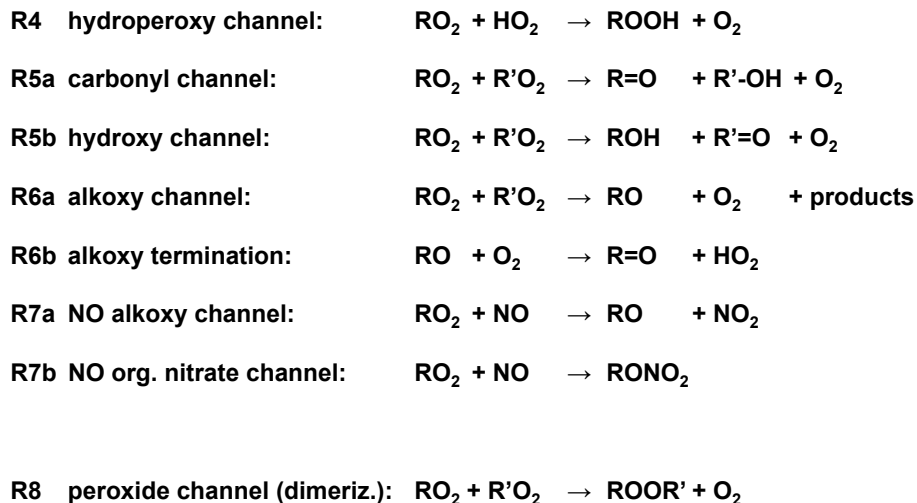
Sequence 2. General RO_2 reactions.
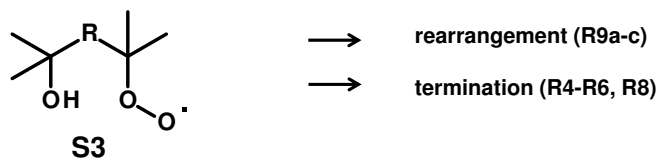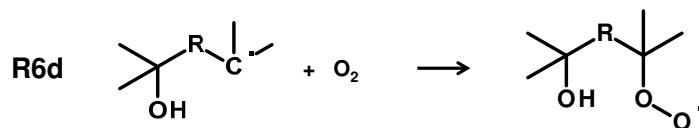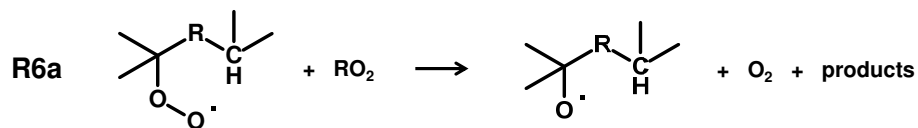
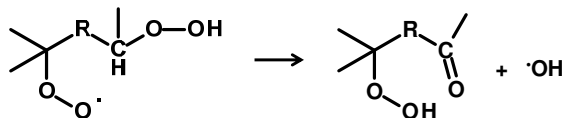**Sequence 3.** Hydroxy-peroxy path via alkoxy channel.

autoxidation pathway

R9a H-shift:
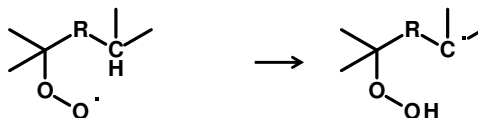
R9b O₂-addition:
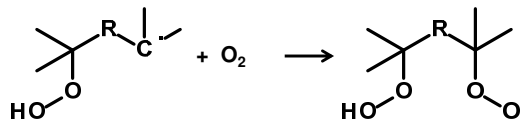
intramolecular termination

R9c carbonyl termination:

Sequence 4. Peroxy path.